ANALYSIS OF INTERNAL COMBUSTION ENGINE CYLINDER BLOCK AND HEAD COOLING USING NANOFLUID COOLANT

by

Kemal Burak Urgancı

B.S., Mechanical Engineering, Uludağ University, 2013

Submitted to the Institute for Graduate Studies in
Science and Engineering in partial fulfillment of
the requirements for the degree of
Master of Science

Graduate Program in Mechanical Engineering

Boğaziçi University

2016

ACKNOWLEDGEMENTS

First, I would like to thank my supervisor Assoc. Prof. Hakan Ertürk for his excellent mentorship throughout my study. I am grateful for his guidance and support. His knowledge, vision, and recommendations made this disseration possible.

I would like to thank all my friends and colleagues in Boğaziçi University for their support and friendship.

Finally, I would like to thank my family for their love, continuous support and encouragement in my whole life, including my graduate study.

ABSTRACT

ANALYSIS OF INTERNAL COMBUSTION ENGINE CYLINDER BLOCK AND HEAD COOLING USING NANOFLUID COOLANT

This study investigates the application of nanofluids in an engine cooling system considering the complete system performance. Performance of nanofluid coolants is examined in comparison with traditional coolants for a 1.5-liter diesel engine cooling system. Pure water, ethylene glycol, and 50% by volume mixture of ethylene glycol and water are considered as basefluids, and nanofluids with CuO, Al_2O_3 and hBN nanoparticles for a particle volume fraction of 0.5-3% range are investigated. System components are modeled individually and the overall cooling performance is investigated for the complete system. As a result, it is shown that Al_2O_3, CuO, hBN-containing nanofluids have superior thermal performance with respect to their corresponding base fluids as coolants. It is also shown that there exist an optimum particle volume concentration that leads to a maximum cooling performance when both increase in heat-transfer and pressure drop is considered with increasing particle volume concentration. The use of nanofluids as coolants introduces opportunities such as increasing cooling capacity, reducing engine body temperature or reducing pumping power.

ÖZET

NANOAKIŞKAN SOĞUTUCU KULLANARAK İÇTEN YANMALI MOTOR SİLİNDİR BLOĞU VE KAPAĞININ SOĞUTMA ANALİZİ

Bu çalışma komple sistem performansını göz önünde bulundurarak bir motor soğutma sisteminde nanoakışkanların uygulanmasını incelemektedir. 1.5 litre dizel motor soğutma sistemi için nanoakışkanların performansları, geleneksel akışkanlar ile karşılaştırmalı olarak incelenmiştir. Baz sıvı olarak saf su, etilen glikol ve etilen glikol-su %50 hacimsel karışımı alınmış, 0.5-3% parçacık konsantrasyonundaki CuO, Al_2O_3, ve hBN nanoakışkanları incelenmiştir. Sistem komponentleri ayrı ayrı modellenmiş ve tüm sistemin genel soğutma performansı incelenmiştir. Sonuç olarak, Al_2O_3, CuO, ve hBN nanoparçacıklarını içeren nanoakışkanların söz konusu baz akışkanlardan daha üstün ısıl performanslara sahip olduğu görülmüştür. Ayrıca ısı transferi ve basınç düşümündeki artış göz önüne alındığında, maksimum performansın elde edilebilmesi için, parça konsantrasyonunun artırımında optimal bir konsantrasyon değerinin olduğu saptanmıştır. Soğutucu sıvı olarak nanoakışkanların kullanılması, soğutma kapasitesini arttırma, motor gövde sıcaklığını azaltma ya da pompalama basıncını azaltma gibi fırsatlar sunmaktadır.

TABLE OF CONTENTS

LIST OF FIGURES

LIST OF TABLES

LIST OF SYMBOLS

A	Area
A_a	Air side area
A_c	Coolant side area
A_e	Actual fractional error
A_f	Fin area
A_{cf}	Fin cross sectional area
C_{max}	Maximum heat capacity ratio
C_{min}	Minimum heat capacity ratio
C_r	Heat capacity ratio
C_p	Specific heat
$C_{p,a}$	Specific heat of air
$C_{p,bf}$	Specific heat of base fluid
$C_{p,f}$	Specific heat of base fluid
$C_{p,p}$	Specific heat of nanoparticle
C_{nf}	Specific heat of nanofluid
D	Dimensionality
D_h	Hydraulic diameter
d_p	Nanoparticle diameter
E	Error estimator of Richardson Extrapolation
f	Friction factor
f_1	Result of fine grid solution
f_2	Result of medium grid solution
f_3	Result of coarse grid solution
f_{exact}	Result of experimental study
F_s	Safety factor
h	Heat transfer coefficient
h_c	Coolant heat transfer coefficient
h_a	Air heat transfer coefficient
J	Colburn factor

k	Thermal conductivity
$k_{b,f}$	Thermal conductivity of base fluid
$k_{n,f}$	Thermal conductivity of nanofluid
k_p	Thermal conductivity of nanoparticle
k_f	Fin thermal conductivity
L_f	Fin length
L_l	Louver length
M	Moleculer weigth
m	Fin parameter
$\dot{m}_a$	Air mass flow
$\dot{m}_c$	Coolant mass flow
N	Avagadro number
N_f	Number of fins
N_s	Number of symetric units
N_1	Number of fine grid nodes units
N_2	Number of coarse grid nodes
p	Order of convergence
P	Peripheral length
P_f	Fin distance
P_l	Louver distance
P_w	Wetted number
Pr	Prandtl number
Pr_a	Air side prandtl number
r	Refinement ratio
R_A	Radiator area ratios
R_{e-a}	System resistance
R_{e-i}	Engine resistance
R_{i-o}	Flow resistance
R_{o-a}	Radiator resistance
R_w	Thermal resistance of tubes
Re	Reynolds number
Re_l	Louver side reynolds number

Q	Volumetric flow rate
Q_c	Coolant volumetric flow rate
T	Temperature
T	Air temperature
T_o	Temperature
t_f	Thickness of fins
U	Velocity
U_a	Air side mean velocity
β	Fraction of liquid volume traveling with a particle
ΔP	Pressure drop
ΔP_{engine}	The coolant pressure drop across the engine
ΔP_{minor}	Pressure drop due to minor losses
$\Delta P_{radiator}$	The pressure drop across the radiator
ΔP_{system}	System pressure drop
ΔQ	Flow rate change
ΔR_{e-a}	System resistance change
ΔT	Temperature change
ΔT_{max}	Maximum surface temperature change
ε	Effectiveness of radiator
η_o	Overall efficiency
η_f	Efficiency of fins
κ	Boltzmann constant
μ_{bf}	Dynamic viscosity of base fluid
μ_{nf}	Dynamic viscosity of nanofluid
π	Pi number
ρ	Density
ρ_a	Air density
$\rho_{,f}$	Density of base fluid
ρ_{nf}	Density of nanofluid
ρ_f	Density of basefluid
ρ_p	Density of nanoparticle

φ	Volume fraction
ψ	Sphericity factorn

LIST OF ACRONYMS/ABBREVIATIONS

3D	Three Dimensional
Al_2O_3	Alumina
CAD	Computer Aided Design
CuO	Copper oxide
EG	Ethylene glycol
EG/W	Ethylene glycol-Water 50% volume mixture
GCI	Grid Convergence Index
hBN	Hexagonal boron nitride
J	Joule
K	Kelvin
kg	Kilogram
l	Liter
m	Meter
mm	Milimeter
NTU	Number of transfer units
Pa	Pascal
s	Second
W	Watt

1. INTRODUCTION

1.1. Problem Overview

Heat transfer plays an important role in engineering applications for many different areas. Heat-transfer improvements continue to excite the attention of the scientists, researchers and industrial companies with the speed of development in science, technology and engineering as well as the competition in scientific and industrial world. Automotive industry, computers and electronics, power plants and reactors, heating systems are common examples of the most important industries, in which heat-transfer has a key role in terms of cooling or obtaining thermal stability. Hence, new methods to increase heat-transfer are analysed continuously.

The importance of heat-transfer efficiency increased significantly, thereby the improvements in the science and technology, as well as the needs of society and optimization of current applications. The quality and thermal performance related properties of the heat-transfer fluid is the limiting factor for the efficiency of most systems, since in most of designs the efficiency of other factors have been maximized. Therefore, the focus has been set on the heat-transfer fluids to increase the heat-transfer efficiency.

Automotive industry is a well known supporter of research and development in a global aspect. Several factors such as competition, customer comfort and needs, laws and regulations, and seeking for more profitable solutions lead to constant search for development and refinement. Therefore, every small case of advantage is considered crucial. Vehicle engines are especially in focus of research and development departments and being the most advanced, complex and important part of commercial and passenger vehicles [1].

Technological advancement and intense competition amongst automobile manufacturers have led to the need and development of high efficiency engines. Internal combustion engines with improved performance and fuel economy had greater heat

produced during operation. Improved rate of heat-transfer is therefore needed to regulate engine surface temperature for optimum efficiency. Automotive engine cooling system takes care of this excess heat produced during engine operation. The primary objective on this branch is to enhance the amount of cooling load for cooling systems in order to increase heat removal from the engine. The availability of higher heat removal can influence system in two ways: improvement in performance with the same system or achieving the same performance with smaller and more compact systems. One major goal in internal combustion engine development is achieving cooling requirements with smaller and lighter cooling systems.

1.2. Motivation

Continuous development in automotive industry has increased the demand for high efficiency engines, not only based on its performance but also for better fuel economy and less emission. There is increasing demand for reducing weight by optimizing design and size of engine block, and all components including cooling system. The shrinking engine sizes lead to engines with higher power per volume leading to increasing heating density that requires improved cooling. Moreover, the internal combustion engine components exposed to the high temperatures inside the engine are subject to high thermal loading during engine operations.

Operating these higher heat density engines without appropriate cooling will lead to an increased engine body temperature, reduced charge coefficient and combustion efficiency. These not only will cause an overall deterioration in the power output, fuel economy, emissions, but also in reliability and durability of the engine [1]. The improved thermal management of engines not only would lead to an efficiency increase, to improve combustion quality reducing the emission of NO_x and other pollutants in the exhausts, it would also prolong the usable life of engine oil and improving engine reliability by reducing friction and abrasion [2]. Alternatively, improved cooling rates for automotive and truck engines can be used to remove more heat from higher horsepower engines with the same size of coolant system [1].

There are several methods for improving the heat discharging capability of the engine. The most commonly used one is to enhance the cooling effect by improving the structure of cooling jacket. Use of more powerful pumps and fans is another commonly adopted method. Another method is using coolants with more efficient heat-transfer capability in the engine cooling system. Heat transfer research has been focusing on the enhancement techniques such as use of higher conductivity additives to the heat-transfer medium. [3] introduced using colloidal suspensions containing of nanometer sized particles that are known as "nanofluids" and significant research has been carried out in regards to nanofluids since then. Nanofluids are prepared by adding an appropriate proportion of nanoparticles into a base liquid through various processes to form a uniform, stable and thermally conductive suspension. It was demonstrated that nanofluids exhibit thermal conductivity enhancement beyond the predictions of various effective medium theories and they are considered as next generation of heat-transfer fluids [4].

Ethylene glycol and water mixtures, which are widely used as automotive coolants, are relatively poor heat-transfer fluids compared to pure water. The performance of engine oils are even worse as a heat-transfer medium. Therefore, there exists be a significant opportunity for improving thermal management in automotive systems using improved conductivity coolants such as nanofluids. The addition of nanoparticles to standard engine coolants has a potential to improve engine cooling rates as addition of nanoparticles changing the transport and heat-transfer characteristics of these coolants.

1.3. Objective and Outline of the Study

In this study, performance of nanofluids in internal combustion engine cooling systems will be investigated in comparison with traditional coolants. Cooling performance of nanofluids with various nanoparticle concentrations is analyzed computationally. Additionaly, common coolants such as ethylene glycol - water 50% volume mixture, pure ethylene glycol, pure water based nanofluids such as Al_2O_3, CuO and hBN will be introduced, and their heat-transfer performance enhancements, pressure

drop characteristics will be compared. Ethylene glycol - water 50% volume mixture is hereafter referred as EG/W. Furthermore, nine different nanofluids comprised of three different nanoparticle materials (Al_2O_3, CuO and hBN) and three different base fluids (EG/W, water, EG) are considered as coolants in this study and a summary of the relations used to predict the thermophysical relations of these nanofluids are presented in comparison to available data.

In the first Chapter, a comprehensive literature survey covering the studies and research subjects on the characteristics, the performace investigations of nanofluids in automotive industrie are executed. This review provides detailed information, results, and conclusions about analysis.

Chapter 2 defines the problem. Modelling strategy of engine cooling system that is comprised of 3 components, engine block, radiatior and pump is considered in this study and introduced in detail. Validation and verification study for 3D flow domain of water jacket is conducted in comparison with experimental data. In order to investigate the effect of using different nanofluid coolants on the performance of heat exchanger analytical complete system is defined.

Cooling performance investigation is completed in Chapter 3. In this chapter, the component and system level thermal performance and pumping power results are presented.

1.4. Literature Review

Although engine cooling is a well established application and industry, performance investigation of nanofluids for engine cooling is a topic that has been recently gaining interest. There are limited number of studies in the literature that directly point out performance in vehicle engine systems.

Saripella [5] modeled the cooling system of a Class 8 truck engine by replacing the standard coolant, EG/W, with nanofluids comprised of CuO nanoparticles suspended

in a base fluid of a EG/W [5]. Results for constant heat load and pumping power showed that engine block temperature was decreased 30% by using nanofluids with 4% particle volume fraction. Whereas for constant engine block temperature and pumping power the cooling capacity was increased 5%. Quantitative results showed that engine horsepower can be increased up to 5%, and coolant pump speed and power can be decreased up to 88%.

Bai [6] used Cu-water nanofluids as heat transfer medium in the water jacket and studied the effect of using nanofluids on heat-spreading capability of the engine [6]. Results showed that the heat-dissipating capacity would increase by 44.1% while the pumping power increase of 6% considering constant flow rate for a particle volume concentration of 5%. Liu *et al.* [7] studied on improving heat load of piston and cylinder liner by applying Cu-water and Cu-oil nanofluids numerically. The results showed that the nanofluids could improve the heat load of piston and cylinder liner. For the both case they found that nanofluids enhance the heat-transfer capability and imrove the heat load contact components and 15 ^{o}C of average temperature drop was reported.

Leong *et al.* [8] studied the application of ethylene glycol based Cu nanofluids in a radiator using correlation based model [8]. The results showed that, overall heat-transfer coefficient and heat-transfer rate in engine cooling system increased with the nanofluids compared to ethylene glycol alone. Also, it is observed that, about 3.8% of heat-transfer enhancement could be achieved with the additon of 2% Cu particles at a constant Reynolds number for air and coolant, respectively. Since, the decrease of flow rate arising from the increase of pressure drop was not considered and the comprisons were made for constant Reynolds number, the results represents an optimistic approach.

Also, Peyghambarzadeh *et al.* [9] investigated cooling performance of automobile radiator with water and Al_2O_3 nanoparticles under turbulent flow [9]. And the experimental results demonstrate that increasing the fluid circulating rate can improve the heat-transfer performace up to 40%. Meanwhile application of nanofluid with low

concentrations can enhance heat-transfer efciency up to 45% in comparison with pure water.

Huminic *et al.* [10] performed an analysis for performance of Cu-ethylene glycol nanofluid through the flat tube of an automobile radiator with plate fins [10]. Investigation comprises inlet temperature and nanoparticle concentration level in the range of 348-368K and 0-2%, respectively. The analysis showed that Nu number increases up to 0.5% concentration. Then it decreases from 1% to 2%. Delavari *et al.* [11] simulated the behavior of water and ethylene glycol based Al_2O_3 nanofluids numerically in turbulent and laminar flow regimes in a flat tube [11]. They studied the effect of nanoparticles, inlet temperatures, and Reynolds number on Nusselt number and pumping power. It is eported that a slightly increase in nanoparticles is resulted in a significant increase, up to 23% for Nusselt number in heat-transfer by nanofluid. The results showed 58.1% power reduction for water based Al_2O_3 nanofluid.

Therefore, this study attempts to numerically investigate the heat-transfer performance of an internal combustion engine cooling system under steady operation including cooling jacket around the cylinders of the engine block and radiator using various nanofluid coolants including EG/W, water, EG based CuO, Al_2O_3 and hBN nanofluids. Investigation is carried out considering the performance of the cooling jacket and the radiator individually besides as a system that is driven by a pump that constitutes a constraint considering the pump's performance curve. Overall performance under different constraints that can be achieved utilizing various operation modes such as considering constant flow rate, heat-dissipation rate or maximum temperature in the engine block are also considered. The optimal particle volume concentration is predicted and the overall performance is compared for CuO, Al_2O_3, and hBN nanofluids with all three base fluids.

2. ENGINE COOLING SYSTEM ANALYSIS

2.1. Problem Statement

One of the major goals in internal combustion engine development is improving current cooling systems and achieving necessary cooling requirements with smaller and lighter cooling systems. The primary objective on this branch is to enhance the amount of cooling load for cooling systems in order to increase heat removal from the engine. The availability of higher heat removal can influence system in two ways: improvement in performance with the same system or achieving the same performance with smaller and more compact systems. There are several methods for improving the heat-discharging capability of the engine. The most commonly used one is to enhance the cooling effect by improving the structure of cooling jacket. Use of more powerful pumps and fans is another commonly adopted method. Another method is using coolants with more efficient heat-transfer capability in the engine cooling system.

Ethylene glycol and water mixtures, which are widely used as automotive coolants, are relatively poor heat-transfer fluids compared to pure water. The performance of engine oils are even worse as a heat-transfer medium. Therefore, there exists a significant opportunity to improve thermal management in automotive systems using improved conductivity coolants such as nanofluids. The addition of nanoparticles to standard engine coolants has a potential to improve engine-cooling rates as addition of nanoparticles changes the transport and heat-transfer characteristics of these coolants. Heat transfer research have been focusing on enhancement techniques such as the use of higher conductivity additives to the heat-transfer medium. It was demonstrated that nanofluids exhibit thermal conductivity enhancement beyond the predictions of various effective medium theories and they are considered as next generation of heat-transfer fluids.

Although engine cooling is a well established application and industry, performance investigation of nanofluids for engine cooling is a topic that has been recently

gaining interest. There are limited number of studies in the literature that directly points out performance in vehicle engine systems. Therefore, this study attempts to numerically investigate the heat-transfer performance of an internal combustion engine cooling system under steady operation including cooling jacket around the cylinders of the engine block and radiator using various nanofluid coolants including EG/W, water, EG based CuO, Al_2O_3 and hBN nanofluids. Investigation is carried out considering the performance of the cooling jacket and the radiator individually besides as a system that is driven by a pump that constitutes a constraint considering the pump's performance curve. Overall performance under different constraints that can be achieved utilizing various operation modes such as considering constant flow rate, heat-dissipation rate or maximum temperature in the engine block are also considered. The optimal particle volume concentration is predicted and the overall performance is compared for CuO, Al_2O_3, and hBN nanofluids with all three base fluids.

2.2. Formulation and Methodology

A 1.5 lt passenger vehicle car cooling system is considered in this study. While a more realistic system have many components, a simplified system that is comprised of 3 components, engine block, radiator and pump is considered in this study as shown in Figure 2.1.

The three dimensional CAD model of the 1.5 lt passenger vehicle diesel engine block including its coolant jacket considered is presented in Figure 2.2. The original CAD model was simplified before a computational model was built by simplifying the features that does not have a significant effect on the hydrodynamic and thermal behavior, to prevent any possible problems regarding numerical simulations such as very high aspect ratio sub-elements that might lead to a numerical instability or high number of sub-elements that would lead to unfeasible computational times.

The coolant follows two parallel paths, one around the cylinders and the other through the cylinder heads. As the coolant enters the block, part of it is immediately transferred to the first cylinder's head. The transfer of coolant towards the second path

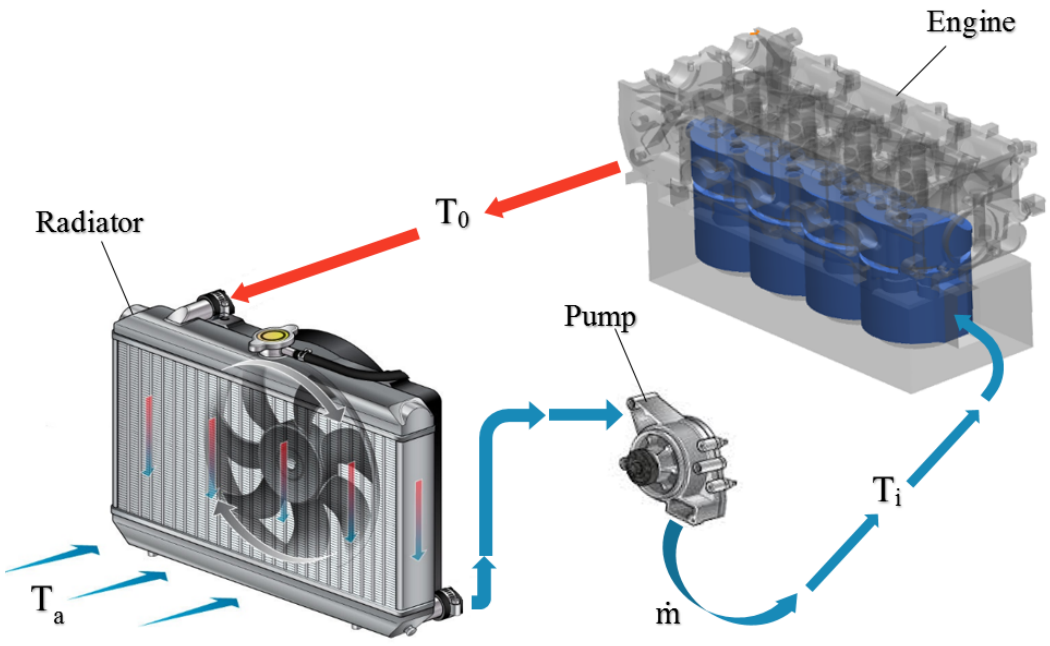

Figure 2.1. Digram of sytem components, coolant flow and temperatures

through the cylinder heat continues as the fluid moves along the first path through two other sets of transfer holes at the end of first and second cylinder s. The coolant flowing through the two paths leave the engine body through two separate exits; one at the end of the main path around the cylinders, and the other at the end of the second path through the heads. The two streams mix outside the engine body. The coolant domain inlet, outlet, the separation and mixing regions are shown in Figure 2.3. The detailed specifications of the engine is presented in Table 2.1.

During operation of an internal combustion engine, only about one-third of the thermal energy released by the fuel is converted into mechanical energy. The remaining two-thirds are released in the form of heat; approximately half of this quantity transported from the engine in the exhaust gas. The remaining energy is taken from the cylinders and cylinder head by the engine cooling system [12, 13]. Thus the heat rejection ratio to the water jacket is nearly same with the utilized energy from the combustion of the gas. Since the engine at issue has 59 kW power output, as it is seen in Table 2.1, heat rejection can be taken same as this amount.

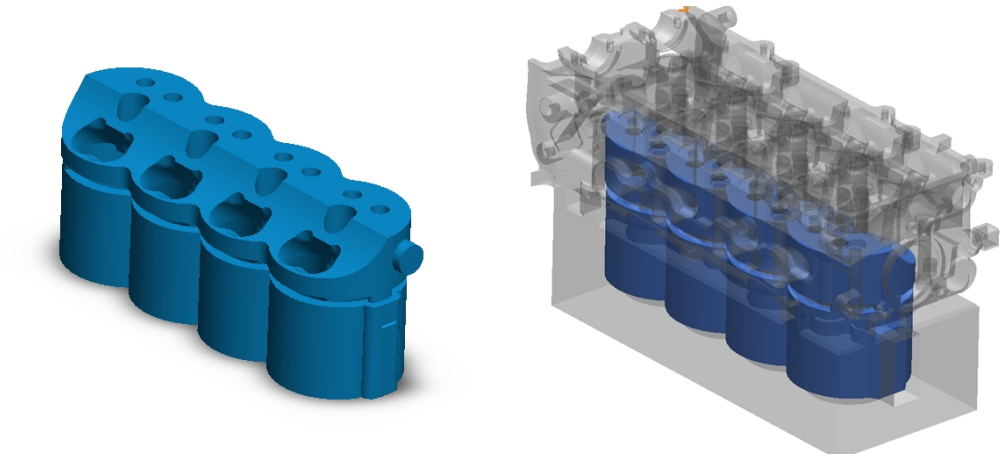

Figure 2.2. Engine block and the coolant flow domain

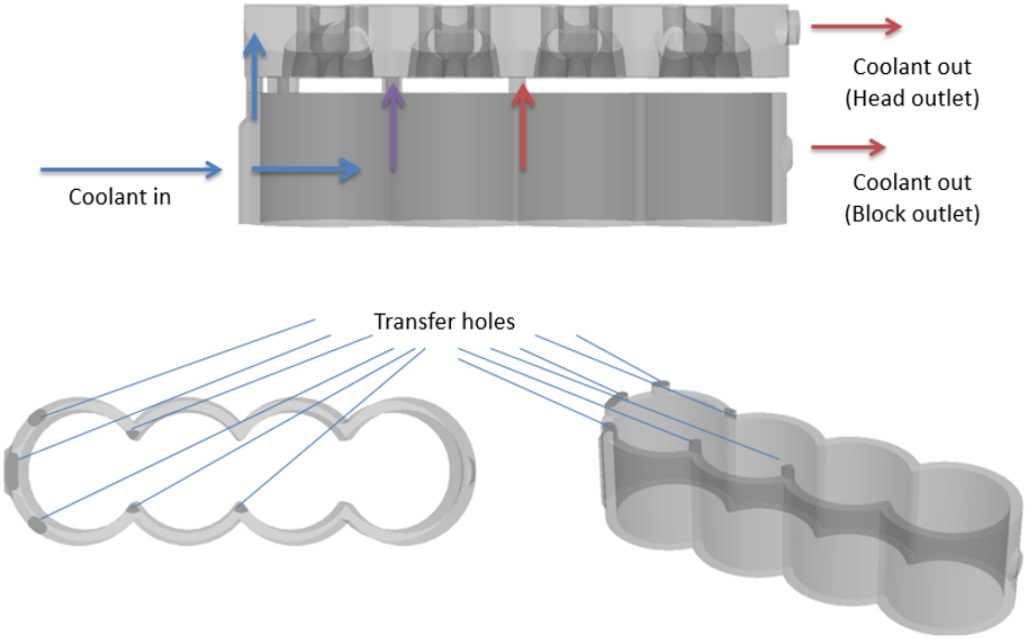

Figure 2.3. Coolant transfer regions

The radiator of the diesel engine cooling system, which is a single pass cross-flow compact heat exchanger with both fluids unmixed, has core dimensions of 694.5 x 462 x 25 mm is considered for the performance analysis. The compact heat exchanger consists of 28 flat tubes and 620 corrugated fins with cross section dimensions of 1.5 x 25 mm and 0.12 mm thickness are used between tubes [14]. The detailed specifications of the radiator is presented in Table 2.2. The radiator is a single pass radiator with continuous parallel liquid tubes and perpendicular air channels in between, separated from each other by fins. The radiator is designed with proper size for a large sized passenger car. The coolant flow through the cooling system is controlled primarily

Table 2.1. Engine specifications [15]

Engine		K9K 1.5 lt Diesel	
Displacement	1461cc	Fuel flow rate	35.74 mg/str
Cylinder bore	76 mm	Inlet port	260 cm^2
Piston stroke	80.5 mm	Exhaust port	90 cm^2
Cylinder wall thickness	8 mm	Piston head	70 cm^2
Rated power @3500 rpm	59 kW	Liner area	1.95 cm^2
Heat rejection @3500 rpm	30%	Cylinder head area	47.75 cm^2

by the operation of the coolant pump. When the pump is driven by the engine, the flow rate is lowered at low engine speed and low heat generation and is higher at high engine speed when larger quantities of heat are developed. The pump is integrated into the housing of the engine block with the hydraulic capacity 1750 mbar pressure and 7500 lt/h flow rate. Characteristic curve of the pump is obtain by fitting a second degree polynomial to the head pressure and the max flow rate as presented in the Figure 2.4.

2.3. System and Component Performance

In order to investigate the effect of using different nanofluid coolants on thermal management a performance metric for the complete system must be defined. A

Table 2.2. Heat exchanger specifications [14]

Core	
Width	694.5 mm
Height	462 mm
Flow direction depth	25 mm
Air flow rate	130 m^3/min
Louver	
Pitch	1.14 mm
Height	0.315 mm
Length	6.74 mm
Angle	28 deg
Fins	
Number of Fins inline	28
Thickness of Fins	0.12 mm
Tubes	
Number of Tubes	2%
Thickness of Tubes	2 mm
Width of Tubes	20 mm
Wall Thickness	0.2 mm

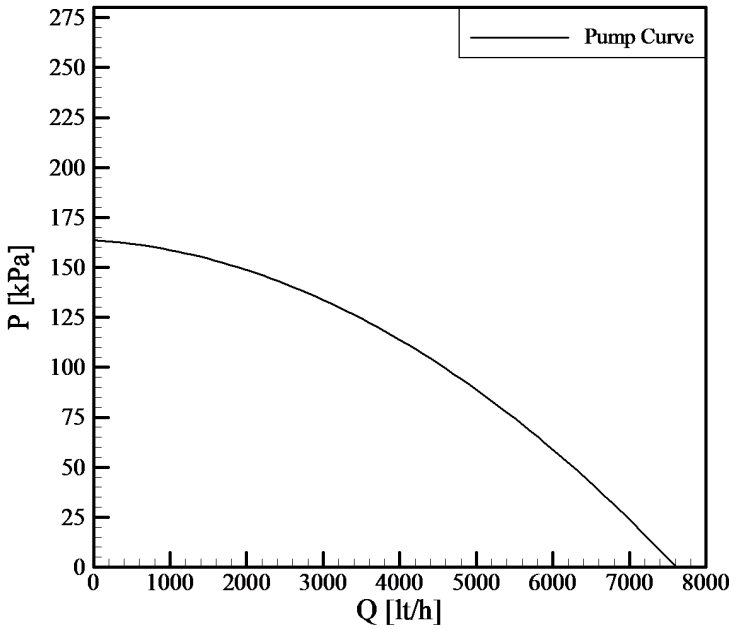

Figure 2.4. Characteristic curve of the pump

reasonable metric to evaluate the thermal performance of the engine cooling system under steady operation is considering the total system thermal resistance that is defined based on the maximum engine temperature, T_e, the ambient air temperature, T_a, and the cooling load, q. The total system resistance or the engine to ambient resistance can then be defined as follows

$$R_{e-a} = \frac{T_e - T_a}{q} \tag{2.1}$$

The total system resistance comprises or three resistances representing the main components as follows

$$R_{e-a} = R_{e-i} + R_{i-o} + R_{o-a} \tag{2.2}$$

Here R_{e-i} and it is defined as follows

$$R_{e-i} = \frac{T_e - T_i}{q} \tag{2.3}$$

where Ti is the coolant inlet temperature to the engine block. The engine block resistance is predicted by estimation of the maximum temperature over the engine block using numerical simulations carried out utilizing the engine model explained earlier for a specified cooling load and coolant inlet temperature as boundary conditions. The details of the numerical models are presented in the next section. The flow resistance, R_{i-o}, represent defined as follows

$$R_{i-o} = \frac{T_o - T_i}{q} = \frac{1}{\dot{m}_c c_{p,c}} \tag{2.4}$$

Here T_o represents the coolant exit temperature from the engine block, and $c_{p,c}$ are the coolant mass flow rate and specific heat, respectively. The flow resistance is usually significantly smaller than the engine block and the radiator resistance for the boundary conditions considered in this study, and it can be neglected. The radiator resistance, R_{o-a}, that is defined based on the inlet temperature of the both fluids can also be defined based on the effectiveness of the heat exchanger, ε, as follows

$$R_{o-a} = \frac{T_o - T_a}{q} = \frac{1}{\varepsilon C_{\min}} \tag{2.5}$$

Here the effectiveness of the radiator, which is a single pass cross flow heat exchanger with both fluids unmixed, can be defined as follows

$$\varepsilon = 1 - \exp\left[\frac{1}{C_{\min}} NTU^{0.22} \left\{\exp\left(-C_r NTU^{0.78}\right) - 1\right\}\right] \tag{2.6}$$

where, the heat capacity ratio is defined as follows

$$C_r = \frac{C_{\min}}{C_{\max}} \tag{2.7}$$

in terms of the minimum heat capacity,

$$C_{\min} = \min\left(\dot{m}_a c_{p,a}, \dot{m}_c c_{p,c}\right) \tag{2.8}$$

and maximum heat capacity,

$$C_{\max} = \max\left(\dot{m}_a c_{p,a}, \dot{m}_c c_{p,c}\right) \tag{2.9}$$

The number of transfer units is

$$NTU = \frac{UA}{C_{\min}} \tag{2.10}$$

where UA is the overall heat-transfer coefficient-area product for the heat exchanger and can be defined based on the overall heat-transfer coefficient-area product of a single symmetric unit $(UA)_s$ and number of symmetric units, N_s, as follows

$$UA = N_s (UA)_s \tag{2.11}$$

where overall heat-transfer coefficient-area product of a single symmetric unit can be defined from the fundamental formulation given as follows

$$\frac{1}{(UA)_s} = \frac{1}{h_c A_c} + R_w + \frac{1}{\eta_o h_a A_a} \tag{2.12}$$

Here, h_c A_c represents the coolant heat-transfer coefficient-area product for a single tube, R_w is the thermal resistance of the tubes, and ha A_a represents the air side heat-transfer coefficient-area product, with the overall surface efficiency, η_o, defined as follows

$$\eta_o = 1 - \frac{A_f N_f}{A_a}\left(1 - \eta_f\right) \tag{2.13}$$

and the efficiency of a single fin can be defined as follows

$$\eta_f = \frac{\tanh\left(mL_f\right)}{mL_f} \tag{2.14}$$

where L_f is the half of the tube-to-tube distance. The fin parameter, m, can be defined as follows

$$m = \sqrt{\frac{h_a P_{w,f}}{k_f A_{c,f}}} \tag{2.15}$$

where fin thermal conductivity, k_f, wetted perimeter and cross sectional area of the fins , $P_{w,f}$ and $A_{c,f}$, respectively. Louvered, corrugated fins are used to enhance air side heat transfer for the radiators. Correlations such as Chang and Wang [16] can be used considering that the numerically modeling the flow through the detailed geometry of louvered, corrugated fins would be computationally demanding. The Stanton number that can be defined as follows

$$St = \frac{h_a}{\rho_a U_a c_{p,a}} = J {Pr_a}^{-2/3} \tag{2.16}$$

where U_a and ρ_a are the air side mean velocity and density, and Pr_a is the Prandlt number of air. The Colburn J factor can be estimated based on the correlation by Chang and Wang [16], as follows

$$\begin{aligned} J = \mathrm{Re}_l^{-0.49}\left(\frac{\theta}{90}\right)^{0.27}\left(\frac{P_f}{P_l}\right)^{-0.14}\left(\frac{L_f}{P}\right)^{-0.29}\left(\frac{D_h}{P_l}\right)^{-0.23}\left(\frac{L_l}{P_l}\right)^{0.68} \\ \times\left(\frac{2L_f}{P_l}\right)^{-0.28}\left(\frac{t_f}{P_l}\right)^{-0.05} \end{aligned} \tag{2.17}$$

where θ is the louver angle, P_l distance between louvers, t_f is the fin thickness, P_f is the fin pitch, D_t is the hydraulic diameter of coolant pipes, L_l is the louver length.

Aside from the thermal analysis, a hydrodynamic analysis must be carried out as the system flow will be adjusted based on the coolant properties. The total pressure

drop in the system is defined as follows

$$\Delta P_{system} = \Delta P_{engine} + \Delta P_{radiator} + \Delta P_{minor} \tag{2.18}$$

The coolant pressure drop across the engine, P_{engine}, is calculated by numerical model considering the difference of the inlet and the outlet pressures in water jacket for a given coolant flow rate. The pressure drop across the radiator, $\Delta P_{radiator}$, is estimated using standard correlations considering nanofluid as single phase homogeneous medium. The pressure drop due to minor losses considering threaded bends, sudden and gradual expansions, and thermostat, P_{minor}, is calculated and considered as of summation of engine and radiator pressure drop values approximately in sequent cases. Once the pressure drop is known, the pumping power can be defined based on the volumetric flow rate, Q_c, as follows

$$W_{pump} = \Delta P Q_c \tag{2.19}$$

2.4. Numerical Analysis of Engine Block

The hydrodynamic and thermal analysis of nanofluid flow within the engine block are carried out via numerical modeling as explained in the previous section. Convective heat transfer with nanofluids canbe modeled using the two phase or single phase approaches. Two phase models provide the possibility of understanding the functions of both the fluid phase and the solid particles in the heat-transfer process. Single phase approach assumes that the fluid phase and particles are in thermal equilibrium and move with the same velocity. There is an ongoing debate on the accuracy of two phase and single phase models for turbulance convection problems. Akbari [17] compared both models of nanofluid turbulent forced convection in a horizontal tube with uniform wall heat flux in comparison with experimental data. It was shown that the results calculated by two phase model are overestimated. Moreover, as the concentration of nanoparticles increases, the predictions by two phase models start diverging from experimental measurement. On the other hand, the results from the single phase model

captures the difference and are in better agreement with the experimental results [17]. Nanofluid convection problem is solved using single phase homogeneous model herein, since the single phase approach is simpler and more conservative. Additionally, computational time requirement is more less while being capable of producing solutions with reasonable accuracy as it is reported in the literature that for turbulent flows [18, 19]. Momentum, energy, and continuity equations are solved using effective nanofluid properties that is considered as incompressible using single phase homogeneous model as explained in [20] and [21].

The numerical solution is carried out based on finite volume discretization using a commercial software (Ansys Fluent^{TM}) to be able to import the engine model from its CAD model. A second order upwind scheme is used for discretization with Semi Implicit Method of Pressure Linked Equations - Consistent (SIMPLEC) algorithm for velocity- pressure coupling. A convergence criterion of $1x10^{-6}$ is used for residuals of all equations. The turbulence in the flow is modeled using a standard $k-\varepsilon$ two equation model considering a turbulence intensity of 5%.

The considered boundary conditions are obtained from an in-cylinder experiment for a diesel spray engine [15]. A uniform heat flux is considered over the cylinder walls, representing the averaged value that is presented in Table 1 as performance of cooling system under steady operation. Therefore, a uniform heat flux boundary condition of 522 kW/m^2 is considered for cylinder walls and cylinder heads, which represents the generated heat at 3500 rpm. The exhaust and intake valves are considered to be at constant temperatures of 910 K and 340 K, respectively. While the coolant inlet temperature to engine block is considered to be 353 K, its exit pressure is considered as atmospheric.

The temperature and pressure distribution in the flow field and temperature distribution over the engine block are predicted through the analysis of the engine block for a given coolant flow rate. The engine block thermal resistance, defined in Equation 2.3 is predicted based on the imposed boundary conditions and estimated temperature distribution. Similarly, the pressure drop along the coolant pathway is

predicted based on estimated inlet pressure.

2.5. System Operating Point and System Performance

The operating flow rate will differ for each coolant due to changing thermophysical properties. For each coolant, all system components are analyzed for three flow rates, 150, 165 and 180 lt/min, to find the operating flow rate. Considering the estimated system pressure drop values for 4 flow rates, the 3 flow rates mentioned above and no flow condition, the system pressure drop can be represented in terms of a second degree polynomial of volume flow rate. The system operating flow rate can then be predicted by equating system pressure drop with pump characteristic curve for each coolant considered. The component and system level thermal performance and pumping power can then be estimated using the system operating flow rate.

2.6. Thermophysical Properties of Nanofluids

Nine different nanofluids comprised of 3 different nanoparticle materials (Al_2O_3, CuO and hBN) and 3 different base fluids (water, EG, EG/W) are considered as coolants in this study. Effective thermophysical properties of these nanofluids are required as single phase homogeneous model will be used in this study. The accuracy of these effective properties have a significant effect on the prediction accuracy. Therefore, a summary of the relations used to predict the thermophysical relations are presented in comparison to available data to be able to interpret the outcomes more clearly.

Base fluid and its thermal and physical properties are effective on the thermal properties of the whole suspension. Therefore, thermal property of the base fluid gives is the lower limit of the nanofluid. Since the water has superior thermal properties than ethylene-glycol and its mixture, it has been expected that nanofluids that use these fluids as base fluid are expected to have thermal properties under the limit of these fluids.

2.6.1. Thermal Conductivity

By definition, thermal conductivity is a significantly important influencing factor for thermal performance of the nanofluids. In a system, thermal conductivity and heat convection of the working fluid are high and the power requirement of the system is low. In general it is observed that the nanoparticle addition increases the thermal conductivity exceptionally.

There are many experimental and theoretical studies investigating the thermal conductivity of nanofluids. Correlations taking different characteristics into account have been proposed to calculate the thermal conductivity of collodial suspensions by Maxwell, Hamilton & Crosser, Xue and Yu & Choi [22]. Maxwell correlation have been driven to calculate the collodial suspensions of normal size, and give relatively low and inaccurate results for nanofluids, underestimating the thermal conductivity enhancement. Maxwell correlation is one of the oldest and the most commonly used model for estimation of the thermal conductivity of collodial suspensions in literature. It simply estimates the thermal conductivity of the nanofluid by the thermal conductivities and volume fractions of the components.

The effective density and specific heat of the nanofluids are calculated using classical mixture theory as follows

$$k_m = \frac{k_p + 2k_b + 2\left(k_p - k_b\right)\varphi}{k_p + 2k_b - 2\left(k_p - k_b\right)\varphi} k_b \tag{2.20}$$

where k_m represents ther thermal conductivity of the nanofluid, k_b is the thermal conductivity of the base fluid, and k_p is used for the thermal conductivity of the nanoparticle phi is used for particle volumetric concentration. Bruggeman correlation [23] also takes the interactions among randomly distributed particles into account.

$$\varphi \frac{k_p - k_m}{k_p + 2k_m} + (1 - \varphi) \frac{k_b - k_m}{k_b + 2k_m} = 0 \tag{2.21}$$

Both Maxwell and Bruggeman theories are general effective medium theories. They are used to decribe distinct cases. Hamilton & Crosser model [24] is developed for more accurate estimations for liquid-solid mixtures containing non-spherical particles considering the fact that thermal conductivity increase cannot be attributed to particle concentration only within the liquid media. The effect of the particle shape is represented in the correlation by introducing a shape factor n which is denotes the shape factor of the particles and defined as n= ψ 3. ψ is the sphericity factor . Hamilton Crosser model is an extension of Maxwell's theory, accounting for the nonsphericity of the particles. Spherical particles have a sphericity $\psi = 1$, leading a shape factor of n=3

$$k_m = \frac{k_p + (n-1)\,k_b - (n-1)\,(k_b - k_p)\,\varphi}{k_p + (n-1)\,k_b + (k_b - k_p)\,\varphi} k_b \tag{2.22}$$

In the past decade, there have been many experimental as well as numerical studies to explore the advantages of nanofluids under variety of conditions. Koo and Kleinstreuer [25] presented a thermal conductivity model , Equation 2.23, which takes into account the effect of particle size, particle volumetric concentration, temperature and properties of base fluid as well as nanoparticles subjected to Brownian motion.

There are many experimental and theoretical studies in the literature investigating the change in the thermal conductivity and viscosity of nanofluids with different particle materials and base fluids. Koo and Kleinstreuer [25] presented a thermal conductivity model that considers the effect of particle size, volumetric concentration, and properties of base fluid, considering temperature dependence due to Brownian motion based on experimental data for Al_2O_3 and CuO nanofluids [25].

$$k_{nf} = \frac{k_p + 2k_{bf} + 2\,(k_{bf} - k_p)\,\varphi}{k_p + 2k_{bf} + (k_{bf} - k_b)\,\varphi} k_{bf} + 5x10^4 \varphi \rho_{bf} c_{p,bf} \beta\,(\varphi) \sqrt{\frac{k_B T}{\rho_p d_p}} f\,(T, \varphi, etc.) \tag{2.23}$$

where β represents the friction of the liquid volume which travels with a particle and decreases with the particle volumetric concentration because of the viscous effect of moving particles. Since the dependence of thermal conductivity on temperature is weak, they introduced an empirical function f(T, φ) using the experimental data of

Das *et al.* [4] on CuO nanofluids.

Vajjha and Das [26] analyzed several existing thermal conductivity models and compared them against their experimental data. They found that the correlation given by Koo and Kleinstreuer. However, the correlation of Koo and Kleinstreuer is based on a limited amount of data obtained from experiments on nanofluids over the temperature range 293K T 325K and concentration range 1%<φ <4%. Therefore, they proceeded to improve this model by deriving new empirical correlations for β and f(T, φ) from their experimental data. The thermal conductivity model remains the same but new correlations derived from broader set of data its valid for the temperature range of 298K <T <363K and the concentration range of 1% <T <10%.

$$k_{nf} = \frac{k_p + 2k_{bf} + 2\left(k_{bf} - k_p\right)\varphi}{k_p + 2k_{bf} + \left(k_{bf} - k_b\right)\varphi} k_{bf} + 5x10^4 \varphi \rho_{bf} c_{p,bf} \beta\left(\varphi\right) \sqrt{\frac{k_B T}{\rho_p d_p}} f\left(T, \varphi\right) \tag{2.24}$$

$$f\left(T, \varphi\right) = \left(2.8217x10^{-2}\varphi + 3.917x10^{-3}\right)\left(\frac{T}{T_o}\right)\left(-3.0669x10^{-3}\varphi + 3.9112x10^{-3}\right) \tag{2.25}$$

where the first term represents effective medium theory based static contribution and the second term represents the contribution of Brownian motion. The empirical function $f(T, \varphi)$ can be defined as and the other empirical function $\beta(\varphi)$ represents the fraction of the liquid that travels with a particle due to viscous effects and is defined as presented in Table 2.3. Since the correlation derived by Vajjha is valid for broader range of temperature, conductivity of Al_2O_3 and CuO nanofluids estimated using this correlation. A comparison among several correlations and experimental data for CuO nanoparticles is shown in Figure 2.5.

Table 2.3. Curve fit relations for proposed $\beta(\varphi)$ function

Particle	$\beta(\varphi)$	**Concentration[%]**	**Temperature[K]**
Al_2O_3	$8.4407(100\varphi)^{-1.07304}$	1$\leq \varphi \leq$10	298$\leq$ T$\leq$363
CuO	$9.881(100\varphi)^{-0.9446}$	1$\leq \varphi \leq$6	298$\leq$ T$\leq$363

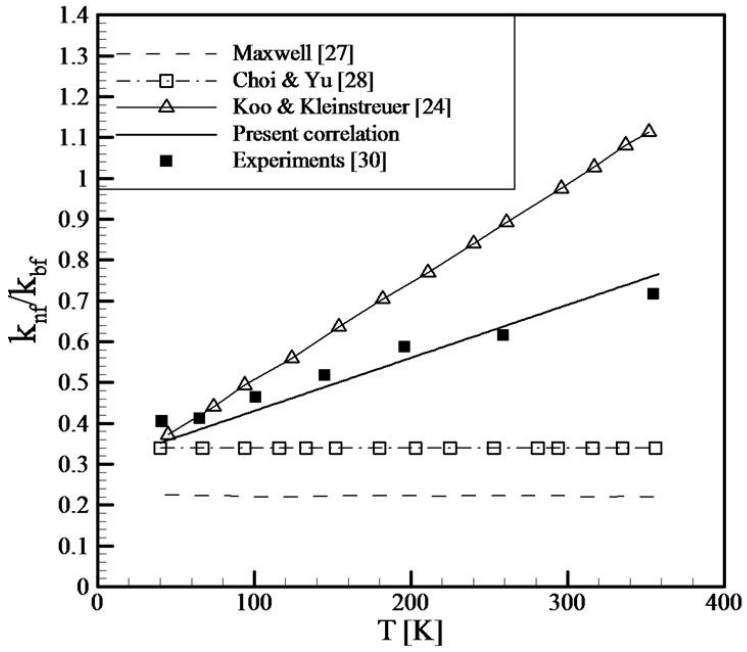

Figure 2.5. Comparison between several theoretical models and experimental data on thermal conductivity

Thermal conductivity of hBN nanofluids are calculated based on experimental data presented in İlhan *et al.* [27]. Since the experiments were conducted for 25^oC, temperature dependency of thermal properties are considered constant and properties were designated over based fluid temperature dependent properties using increment presented in the paper.

Figure 2.5 shows the comparison of Eqs. 2.24 and 2.25 with the experimental data which were collected from an experiment with CuO nanoparticles and the performances of various models . It is observed that Koo and Kleinstreuer model agrees with experimental data up to a temperature of 325 K for which it was developed. Beyond this range the correlation overpredicts the conductivity ratio. The models of Maxwell [28] and Yu and Choi [29] do not show any noticeable increase in thermal conductivity with temperature. As it can be seen from the figure hermal conductivity ratio is able to be estimated from Equation 2.24 for the range of specified temperature and nanoparticles. Thermal conductivity ratios of three nanofluids based on three different based fluids are presented from Figure 2.7 to Figure 2.11.

2.6.2. Viscosity

The heat-transfer performance can be increased by thermal conductivity enhancement, similar effect can also be observed for viscosity. The pumping power required for a given flow rate is expected to increase as the viscosity increases. Therefore, depending on the system specifications, a reduction of flow velocity could result in detraction the benefit of thermal conductivity enhancement. Temperature has an inherent relation with viscosity. As the temperature increases, intermoleculer attraction between the nanoparticles and their base fluids weakens. Hence, the viscosity of the nanofluids decreases with the increase in the temperature.

First conventional model to formulate the effective viscosity of solid-liquid mixtures with spherical particles was proposed by Einstein [30] as follows

$$\mu_{nf} = (1 + 2.5\varphi)\,\mu_{bf} \tag{2.26}$$

where μ_{nf} and μ_{bf} is the viscosities of mixture and the base fluid, respectively. According to the theory, the viscosity of the suspension is linearly dependent on only particle concentration. Another model is stated by Brinkman [31] and it suggests that effective viscosity can be defined as the power of volume concentration as follows

$$\mu_{nf} = \left(\frac{1}{1-\varphi^{2.5}}\right)\mu_{bf} \tag{2.27}$$

Both theoritical models only use the concentration to estimate the viscosity. However, studies shows that several different parameters, such as particle size and shape, temperature of the medium, specific interface interactions between nanoparticles and base fluids [32].

Besides theoritical models, Corcione [33] developed empirical model by using a large number of experimental data which includes the effect of base fluid type on the

change of viscosity as follows

$$\frac{\mu_{nf}}{\mu_{bf}} = \left(\frac{1}{1 - 34.87(d_p/d_f)^{-0.3} \varphi^{1.03}} \right) \tag{2.28}$$

where d_f is the equivalent diameter of a base fluid molecule, defined as follows

$$d_f = \left(\frac{6M}{N\pi\rho_{bf}} \right)^{1/3} \tag{2.29}$$

in which M is the molecular weight of the base fluid, N is the Avagadro number and ρ_{bf} is the mass density of the base fluid calculated at temperature of T_0=293 K.

Since there are many equations reported by researches based on temperature dependency of viscosity most of them carried out for narrower temperature range [34]. A general correlation for viscosity in between considered temperature range was developed by Vajjha *et al.* (2008) [26] is defined as in the Equation 2.30 and the curve fit relations for the terms of the correlation is presented in the Table 2.4 [35].

$$\frac{\mu_{nf}}{\mu_{bf}} = A_1 e^{(A_2 \varphi)} \tag{2.30}$$

While there are many experimental studies in regards to thermophysical properties of

Table 2.4. Curve fit relations for proposed viscosity relation in Equation 2.30

Nanoparticles	$\mathbf{A_1}$	$\mathbf{A_2}$	**Avg.Par.Size**[μ**m**]	**Concentration**[%]
Al_2O_3	0.983	12.959	45	0< φ <0.1
CuO	0.9197	22.8539	29	0< φ <0.06

Al_2O_3 and CuO nanofluids, studies in regards to hBN are rather limited. In their recent study, Ilhan *et al.* [36] presented the thermophysical properties of hBN nanofluids with water, EG and EG/water as base fluid at room temperature. The experimental data presented in that study is used here, considering the temperature dependent properties based on temperature dependent properties of base fluid. Characteristics

of nanoparticles used in this study is presented in Table 2.5. Viscosity ratios of three nanofluids based on three different based fluids are presented from Figure 2.7 to Figure 2.11.

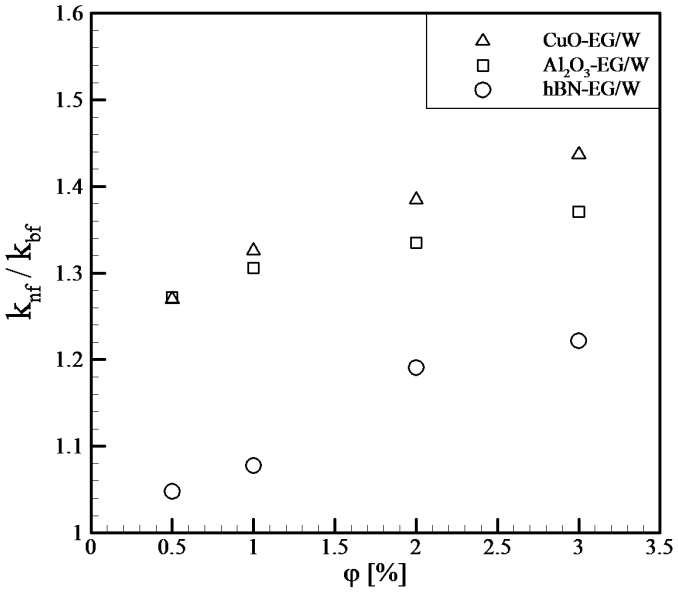

Figure 2.6. The comparison of EG/W based nanofluid thermal conductivity changing with particle volume fraction

2.6.3. Density and Specific Heat

The effective density and specific heat of the nanofluids are calculated using classical mixture theory as follows

$$\rho_{nf} = (1-\varphi)\,\rho_f + \varphi\rho_p \tag{2.31}$$

$$c_{nf} = \frac{(1-\varphi)\,\rho_f c_{p,f} + \varphi\rho_p c_{p,p}}{\rho_{nf}} \tag{2.32}$$

where φ represents the particle volume fraction and subscripts n_f, p, and f, identify quantities for nanofluid, particle and base fluid, respectively. The properties for the

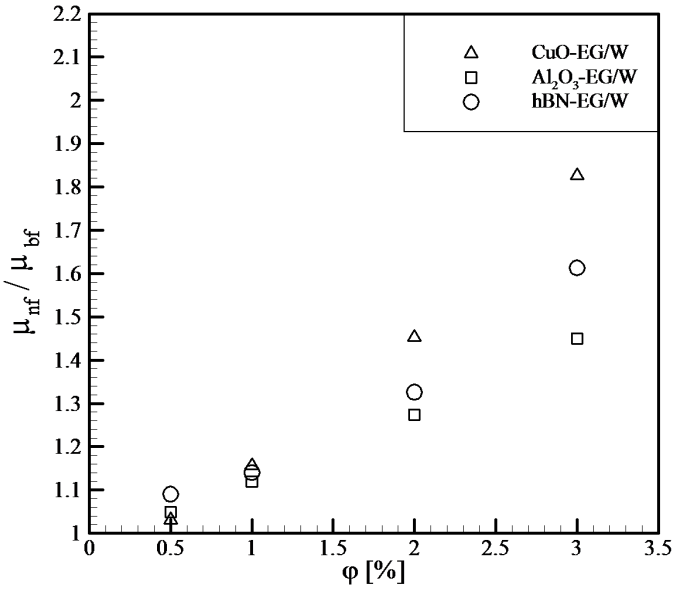

Figure 2.7. The comparison of EG/W based nanofluid viscosity changing with particle volume fraction

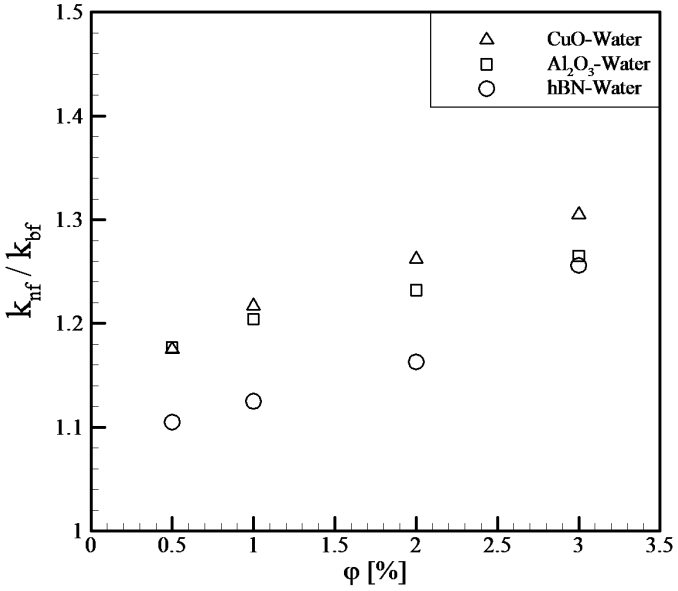

Figure 2.8. The comparison of water based nanofluid thermal conductivity changing with particle volume fraction

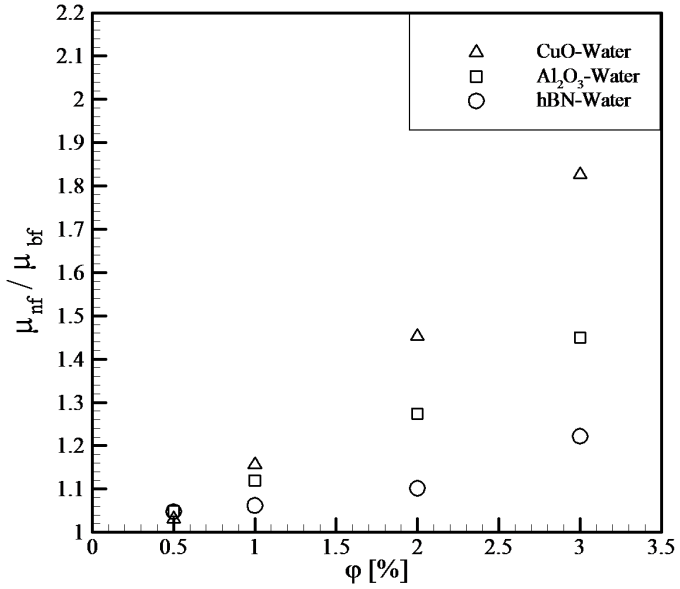

Figure 2.9. The comparison of water based nanofluid viscosity changing with particle volume fraction

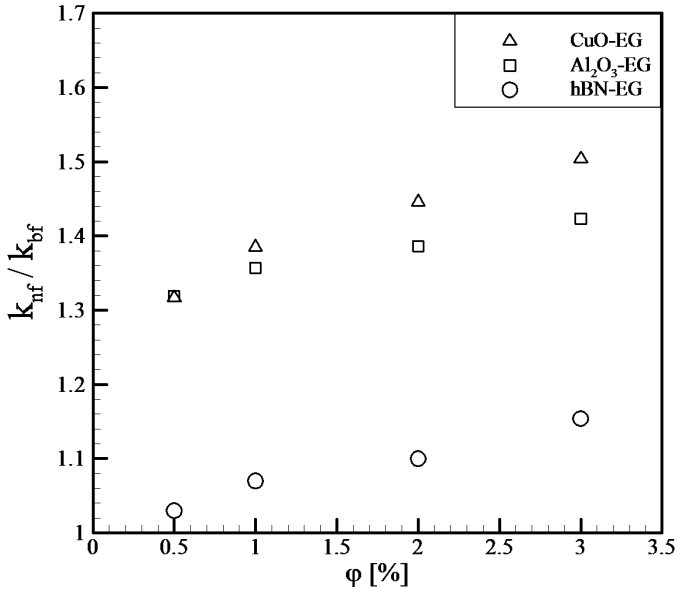

Figure 2.10. The comparison of EG based nanofluid thermal conductivity changing with particle volume fraction

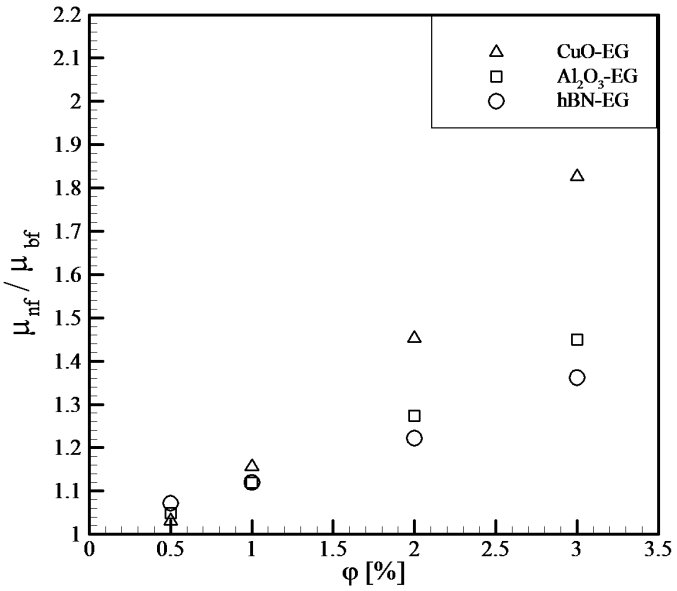

Figure 2.11. The comparison of EG based nanofluid viscosity changing with particle volume fraction

nanoparticles considered in this study are presented in Table 2.5. Temperature dependent thermal properties of base fluids are obtained from literature [37]. Temperature dependent thermal conductivity and viscosity of EG/W based nanofluids are presented in Appendix C.

Table 2.5. Characteristics of nanofluids used in this study

Particle	**Density[kg/m^3]**	**Part. Dia.[μm]**	**Ther. Conduc.[W/mK]**
Al_2O_3	3600	45	36
CuO	6500	29	17.65
hBN	2200	29	13

3. RESULTS AND DISCUSSIONS

3.1. Validation of Flow Geometry

All discrete methods introduce discretization error which arises from the use of finite number of the grid points. As the grid cells become smaller and the number of cells in the flow domain increase the grid discretization error, should asymptotically approaches zero. Grid refinement study is a common approach used in assessing numerical accuracy of a simulation [38]. Simulations with different mesh resolution have been evaluated and compared to ensure that results are grid independent.

In order to test the validity and precision of the simulationsIn order to test the reliability of refined mesh, a grid independence study is carried out to identify the adequate grid resolution using GCI method. GCI method and the process of the validation study is explained in detail in Appendix A. Solutions with different grid resolutions are run and results are evaluated with theoritical or experimental results from literature. 3 different meshes compared for EG/W base fluid case. Mesh 1 has 2522453 nodes; mesh 2 has 4543665 nodes; and mesh 3 has 5889273 nodes. The highest number of nodes is specified considering geometrical limitations. It was identified that the grid with 4543665 nodes as shown in Figure 3.1 is proper to obtain grid independent results.

This process is accomplished throughout the analysis for each geometrical setup considered. Flow domain geometry is cleaned from unnecessary complications prior to grid generation. If the surface mesh is not sufficiently fine, the geometry will not be simulated realistically. Since our concern is the temperatures of boundaries, in order to procure sufficient flow and temperature results, mesh inflations are applied to the boundaries which are contacting to heat flux. Figure 3.2 shows the the inflated boundary meshes.

Figure 3.1. Meshed flow domain

Validation study is conducted by using the experimental dat from literature. Maximum surface temperatures is compared with the study of Vatandaş [15]. Power output of the engine in the study has been set as boundary condition of surface heat flux of combustion chamber. The fluid is evaluated with constant heat flux heating. Therefore, approximate surface temperature, reported in the study, attempted to obtain. Comparisons have been made over the maximum temperature of the surface temperature of the cylinder head. The results within an reasonable error range are selected, and the one with lowest computational time and effort is chosen.

3.2. System Performance

The system resistance R_{e-a}, is obtained by summing the engine block, flow resistance, and radiator resistances. Pressure drop and thermal resistance calculations are repeated for three different, specified flow rates. Using the calculated system pressure drops for the specified flow rates a compact model for the system pressure drop for the specific fluid can be developed by fitting a second degree polynomial of volume

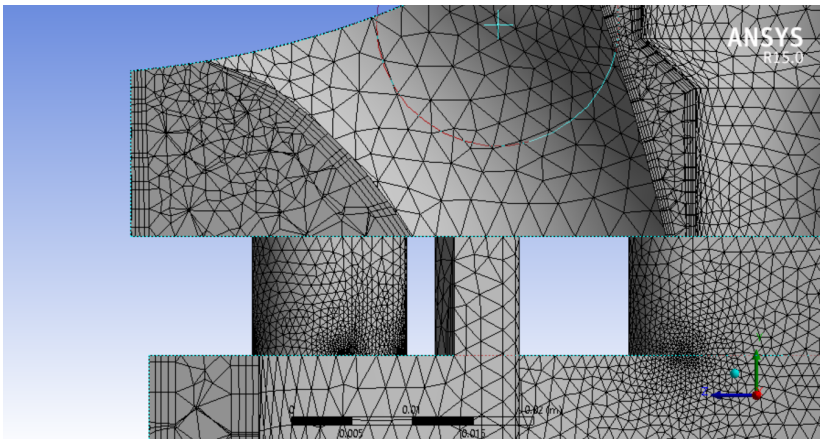

Figure 3.2. Inflations under the domain surface

flow rate. A similar compact model can be developed for the system resistance, by fitting a power function of volumetric flow rate. These compact models are valid for the particular system and particular coolant considered.

The system operating flow rate can then be obtained by intersecting the pump characteristic curve and pressure drop as it is represented in Figure 3.3. The cooling system's performance can be defined in terms of a resistance in Figure 3.2, based on the operating flow rate estimated from Figure 3.3 and Figure 3.4. The operating point was obtained as 1.98 lt/min and the corresponding block resistance, flow resistance, and radiator resistance are 0.416 K/W, 0.00014 K/W, and 0.0107 K/W, respectively. Hence, the system resistance, R_{e-a}, is 0.426 K/W for EG/W base fluid.

3.2.1. Heat Transfer Performance

Figures 3.5 shows the temperature distribution over the engine block for the case where EG/W is used as a coolant at a flow rate of 150 lt/h. The location of the maximum surface temperature is shown in Figure 3.5, where it can be observed that the outlet region has higher temperature. This is due to the fact that the coolant temperature and the wall thickness are higher around the outlet which increase the thermal resistance between cylinder wall and fluid. Velocity distribution that affects the surface temperatures is presented in Appendix B.

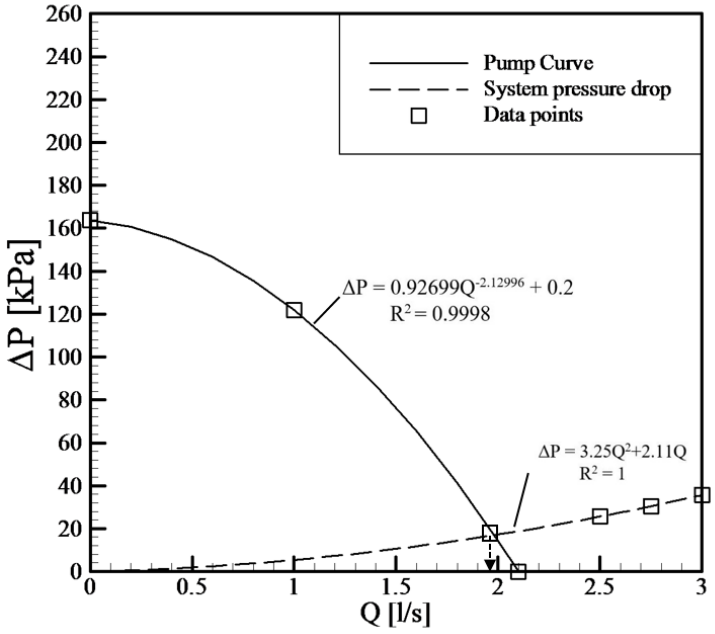

Figure 3.3. Pump curve and System pressure drop intersection for EG/W

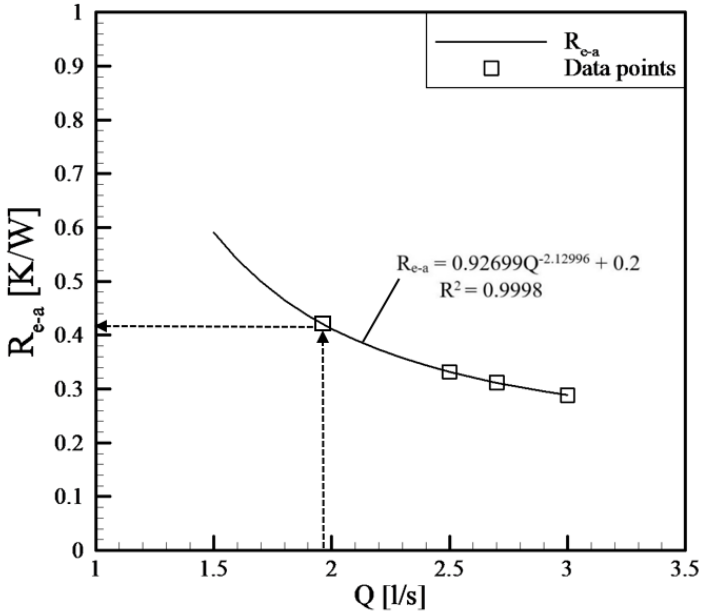

Figure 3.4. System resistance for EG/W

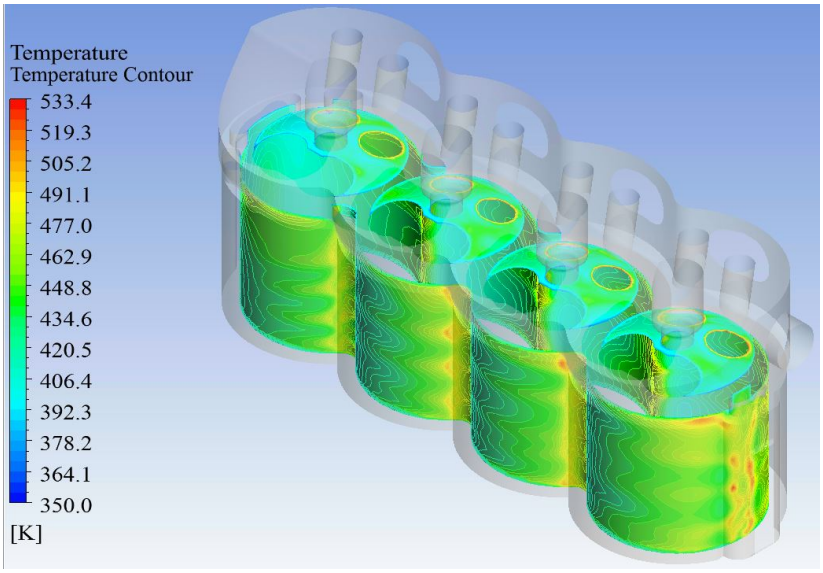

Figure 3.5. Temperature distribution over engine block

Considering that T_{max} and T_a are the design specifications for a particular cooling system, the increase in the cooling capacity can be defined using system thermal resistance as follows

$$\Delta R_{e-a} = 100\frac{q(\phi) - q(0)}{q(0)} = 100\left(\frac{R_{e-a}(0)}{R_{e-a}(\phi)} - 1\right) \tag{3.1}$$

where $q(\phi)$ and $R_{e-o}(\phi)$ represents the cooling capacity and system thermal resistance for a given nanofluid for a particle volume concentration of ϕ. Similarly, for a given cooling load, q, and environmental condition, T_a, the reduction in the maximum engine block temperature is defined as follows

$$\Delta T_{\max} = q\left(R_{e-o}(0) - R_{e-o}(\phi)\right) \tag{3.2}$$

In order to calculate engine block resistance, R_{e-i}, the maximum temperature over the engine block, T_e,, is calculated as 533.4 K and coolant inlet temperature, T_i, is 353 K that is also specified as a boundary condition. Therefore, the block resistance is calculated as 0.342 K/W. In order to calculate the total cooling system's resistance R_{e-a}, is calculated using Equation 2.1. In order to calculate the total cooling system's resistance R_{e-a}, and the total pressure drop ΔP_{system}, radiator side pressure

drop $\Delta P_{radiator}$ is calculated using Equations 2.1 and 2.18. Similar calculation for the radiator side thermal resistance is made using Equation 2.5 to Equation 2.17.

The system resistance R_{e-a}, is obtained by summing the engine block, flow resistance, and radiator resistances. Pressure drop and thermal resistance calculations are repeated for three different, specified flow rates. Using the calculated system pressure drops for the specified flow rates a compact model for the system pressure drop for the specific fluid can be developed by fitting a second degree polynomial of volume flow rate. A similar compact model can be developed for the system resistance, by fitting a power function of volumetric flow rate. These compact models are valid for the particular system and particular coolant considered. The system operating flow rate can then be obtained by intersecting the pump characteristic curve and pressure drop as it is represented in Figure 3.3. and 3.4 The cooling system's performance can be defined in terms of a resistance in Figure 3.3, based on the operating flow rate estimated from Figure 3.4. The operating point was obtained as 1.98 lt/min and the corresponding block resistance, flow resistance, and radiator resistance are 0.416 K/W, 0.00014 K/W, and 0.0107 K/W, respectively. Hence, the system resistance, R_{e-a}, is 0.426 K/W for EG/W base fluid.

The change in cooling system's thermal resistance with respect to the particle volume fraction of the coolant is presented in Figure 3.6. As the particle volume fraction of the coolant increases, the thermal conductivity of the coolant increases leading to a reduction in system thermal resistance. However, the increasing coolant's particle volume concentration also increases the viscosity of the coolant reducing the system's operating flow rate that leads to an increase in the system thermal resistance. As a result of these two opposing effects, there exists an optimal particle concentration, where the resistance is minimum. This point can be clearly observed in Figure 3.6 for all nanofluids in consideration.

The optimal particle volume concentration level is found to be approximately 1% for all EG/W based nanofluid coolants; hence, performances of all nanofluids are compared for this concentration. The highest overall improvement in thermal

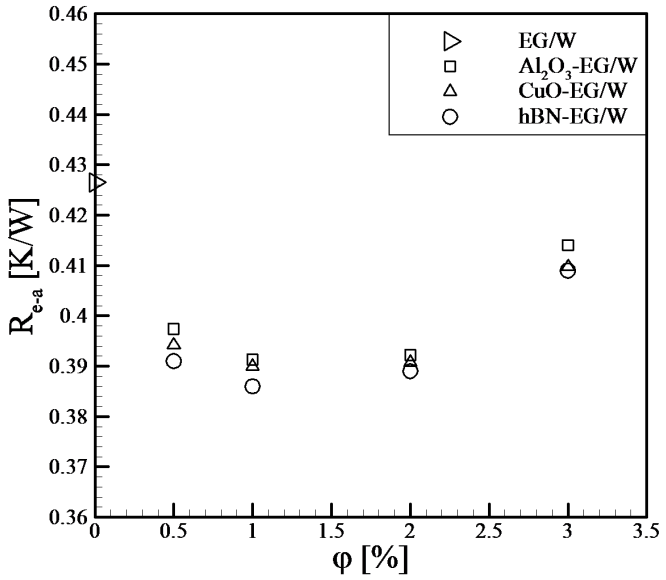

Figure 3.6. System resistance, R_{e-a}, for EG/W based Al_2O_3, CuO, and hBN nanofluids with changing particle volume concentration

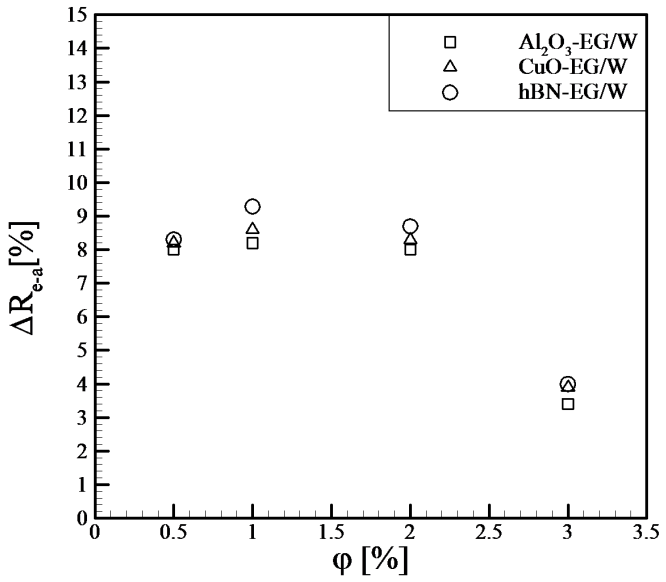

Figure 3.7. System resistance, R_{e-a}, change for EG/W based Al_2O_3, CuO, and hBN nanofluids with changing particle volume concentration coparing with EG/W

performance is observed for hBN nanofluids. System resistance, R_{e-a}, is estimated as 0.386 K/W for hBN nanofluid, while resistances for Al_2O_3 and CuO are 0.392 K/W and 0.39 K/W, respectively. While the differences between thermal resistances for nanofluids coolants are in the third digit, all nanofluids have higher performance than base fluid. The thermal performance of hBN nanofluid coolant is 10.3% higher than it is for pure EG/W coolant. The performance of hBN nanofluid is 1.53% and 1.03% higher than Al_2O_3 and CuO nanofluids, respectively.

The increase in cooling capacity and reduction in maximum engine block temperature is presented in Figure 3.8. As the minimum system resistances are observed for 1% particle concentration of EG/W based nanofluids, the maximum cooling capacity is achieved for the same concentration. The cooling capacity increase for EG/W based Al_2O_3, CuO, and hBN nanofluids are 9.1%, 9.5%, and 10.3%, respectively. The estimated maximum surface temperature reduction for EG/W based Al_2O_3, CuO, and hBN nanofluids are 18 K, 19.3 K, 20.9 K, respectively.

Similar analysis is carried out for cooling capacity of water and EG based nanofluids. The thermal performance of the nanofluids showed similar trends with total system thermal resistance decreases up to approximately 1% particle concentration and then it increases. As a result, the cooling capacity increase maximizes approximately around 1% particle concentration for water and EG based nanofluids as shown in Figure 3.9 and Figure 3.10. The thermal conductivity increase of the water based nanofluids are relatively higher, with relatively less increase in viscosity with increasing particle volume fraction, with respect to that of EG/W or EG based nanofluids. Therefore, the increase in cooling capacity for water based nanofluids is higher than it is for EG or EG/W based nanofluids. This can be observed in Figures 3.7 and 3.8. The maximum cooling capacity increase for water based nanofluids is acquired as 10.9%, 12.1%, and 13% with Al_2O_3, CuO, and hBN nanoparticles, respectively. The increase in cooling capacity for EG based nanofluids with Al_2O_3, CuO, and hBN are 5.3%, 6.5%, and 7.3%, respectively.

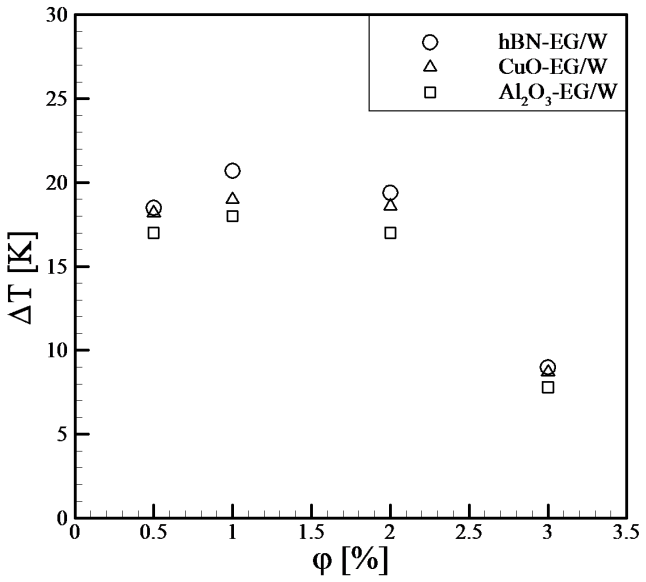

Figure 3.8. Engine block temperatures reductions for EG/W based Al_2O_3, CuO, and hBN nanofluids

Reduction in the maximum engine block temperatures is also estimated and presented in Figure 3.9 and Figure 3.10 for water and Eg based nanofluids, based on the definition presented earlier. The maximum temperature reduction observed in Figure 12 is achieved when using 1% hBN nanoparticles, which is also the case in Figure 10. Here, it should be noted that the maximum engine block surface temperatures when water and EG are used as coolants are 489.8 K and 715.4 K, respectively. While pure water appears as the superior coolant, it should be noted that possible nucleation and phase change is not considered. Reduction in the maximum engine block temperature achieved when EG based nanofluids with 1% particle volume concentration of Al_2O_3, CuO, and hBN nanofluids are 18.4 K, 20.3 K, and 21.8 K, respectively. The corresponding reduction for water based nanofluids are estimated as 18.6 K, 22.4 K, and 24.9 K, for Al_2O_3, CuO, and hBN nanofluids, respectively.

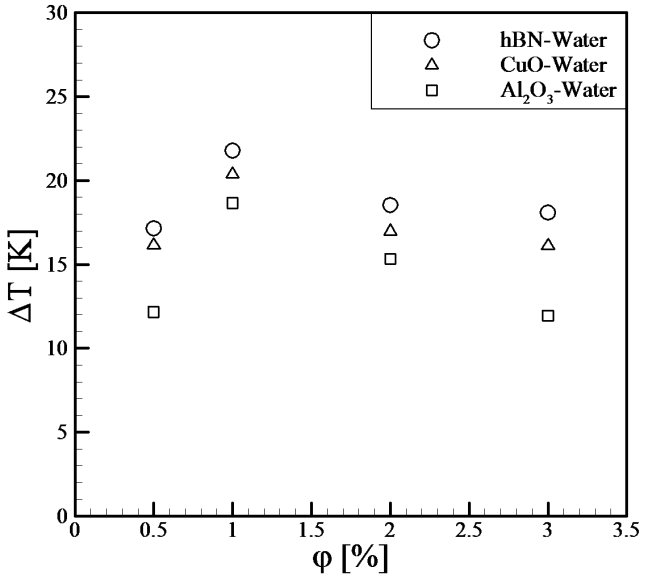

Figure 3.9. Engine block temperatures reductions for Water based Al_2O_3, CuO, and hBN nanofluids

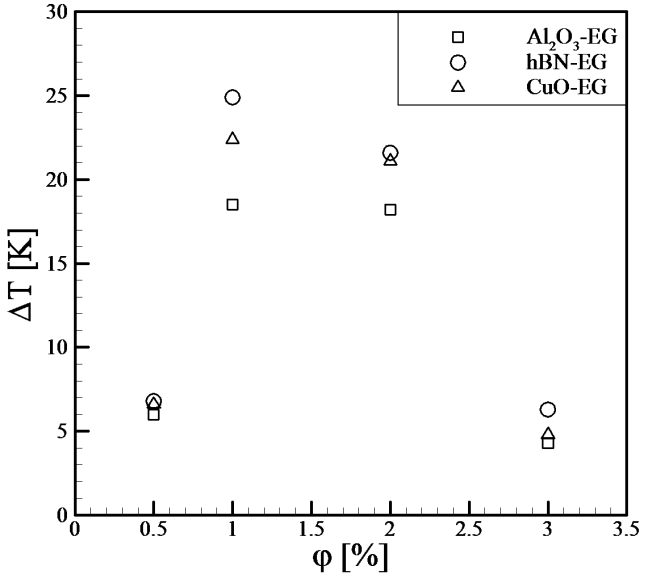

Figure 3.10. Engine block temperatures reductions for EG based Al_2O_3, CuO, and hBN nanofluids

3.2.2. Pressure Drop Calculation and Operating Flow Rate Enhancement

Figures 3.11 shows the pressure distribution over the engine block for the case where EG/W is used as a coolant at a flow rate of 150 lt/h. Pressure drop, ΔP_{engine}, is calculated based on the area averaged inlet and the outlet pressures. The outlet pressure of the water jacket is set to atmospheric pressure and for the case presented in Figure 3.11, the pressure drop is 6.59 kPa.

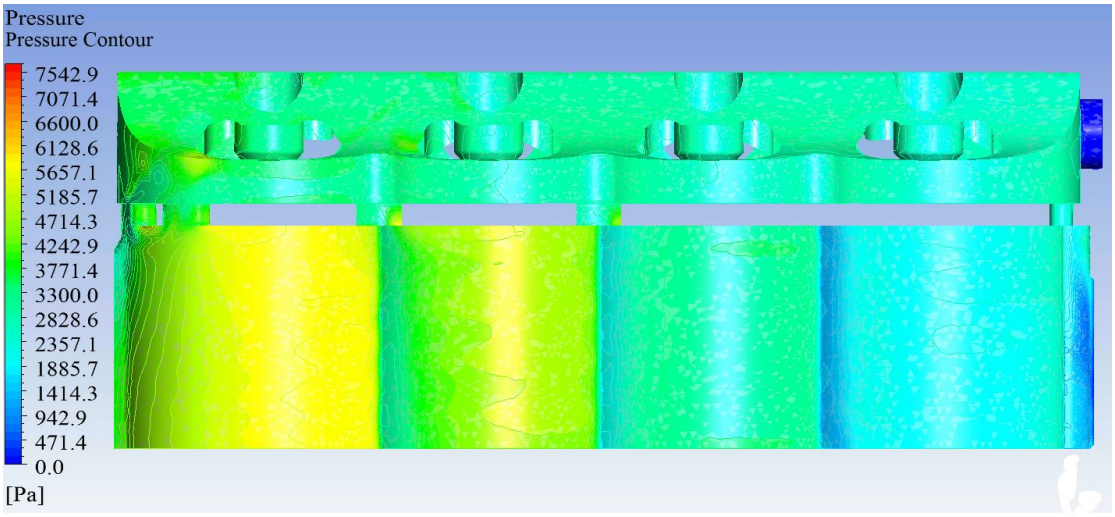

Figure 3.11. Pressure distribution over engine block

In order to calculate the total cooling system's resistance R_{e-a}, and the total pressure drop ΔP_{system}, radiator side pressure drop $\Delta P_{radiator}$ is calculated using Equations 3.3 and 3.4. Similar calculation for the radiator side thermal resistance is made using Equation 2.5 to Equation 2.17.

$$\Delta P_{radiator} = f \frac{L}{D_h} \rho U_m^2 \tag{3.3}$$

$$f = 0.316 \mathrm{Re}_D^{-0.25} \tag{3.4}$$

Considering the pressure distribution over water jacket shown in Figure 3.11, and the estimated pressure drop for radiator, the estimated pressure drops are 6.59 kPa and

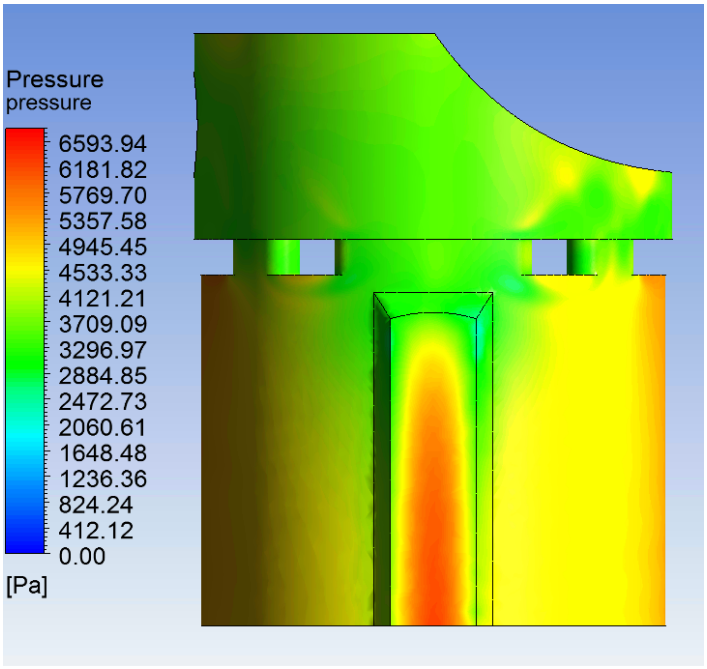

Figure 3.12. Pressure distribution around the inlet of engine block

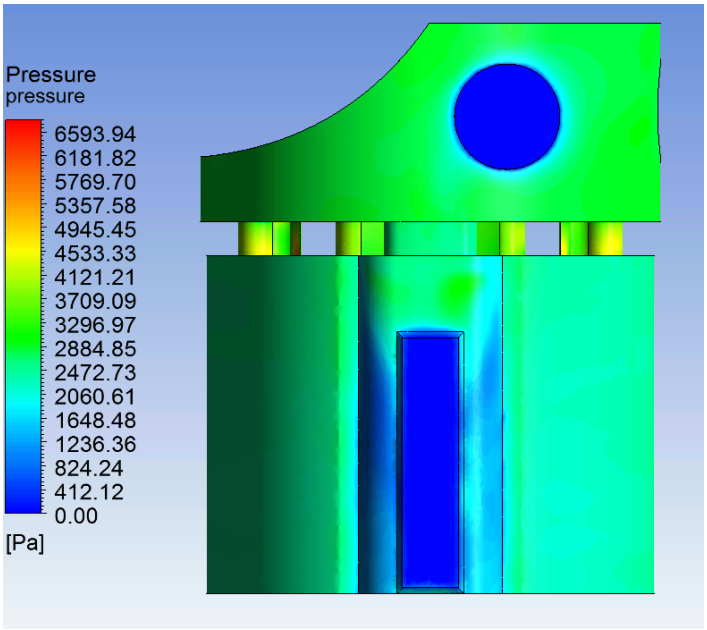

Figure 3.13. Pressure distribution around the outlet of engine block

13.6 kPa, respectively. As it can be seen, flow resistance of the radiator is only a small fraction of the overall system, with engine block being the most dominant component in the system. Therefore, an optimization study to acquire improved cooling performance should focus on engine block rather than the radiator. Moreover, change in pressure drop effects system flow rate and system cooling performance. Since radiator has higher pressure drop, it is more critical to improve radiator performance for enhancing pumping performance and optimize the system flow rate.

Similar analysis is executed for EG/W based Al_2O_3, CuO, and hBN nanofluids of different concentrations, varying between 0.5-3%. While addition of particles increase the viscosity and the density of the fluid, as fluid flows through the coolant path of the cooling jacket, the pressure drop from cooling jacket inlet to outlet increases. As similar effect is also observed for radiator, the addition of nanoparticles increases the system pressure drop, that leads to a reduction in the operating flow rate. Figure 3.14 shows reduction in flow rate using nanofluids with different particle volume concentrations in comparison with the EG/W base fluid. The resulting reduction in operating flow rate for CuO, Al_2O_3, and hBN nanofluids for 1% concentration were obtained as 0.73 lt/min, 0.40 lt/min, and 0.34 lt/min, respectively.

Required flow rates for nanofluid coolants to achieve same maximum engine block temperature, when the base fluids are used as coolants are also estimated. It is observed that with the use of nanofluids, the system can operate on lower flow rates, and nanofluid use has a potential to decrease the pump speed and reduce the pumping power. It is observed that hBN nanofluid with 1% particle concentration has the best combination of properties over the other fluids to achieve reduced flow rate for EG/W, water, and EG as base fluids. Flow rate reductions are 5.6%, 7.1%, and 3.8% for EG/W, water, and EG based hBN nanofluids with 1% particle concentration as observed in Figure 3.15, Figure 3.16, and Figure 3.17.

Additional nanoparticles increase the viscosity and the density of fluids; therefore, it also leads to an increase in pressure drop and pumping power. Figure 3.18, Figure 3.19, and Figure 3.20 show the increment pumping power with the use of nanofluids.

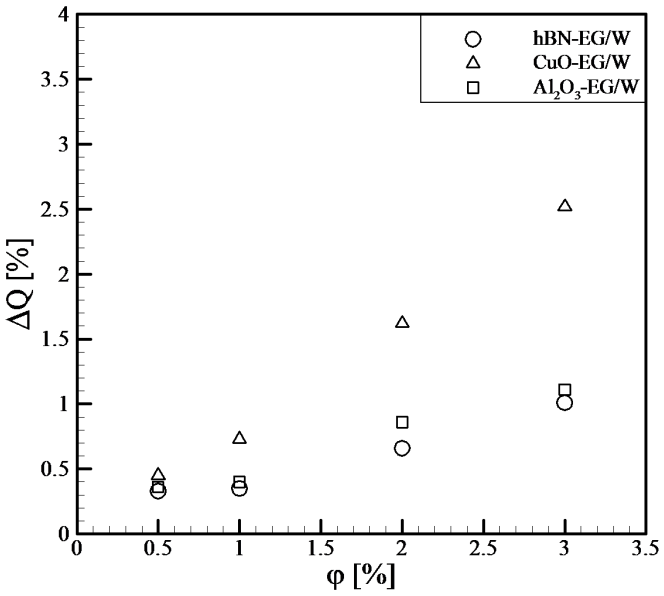

Figure 3.14. Flow rate reductions for EG/W based nanofluids

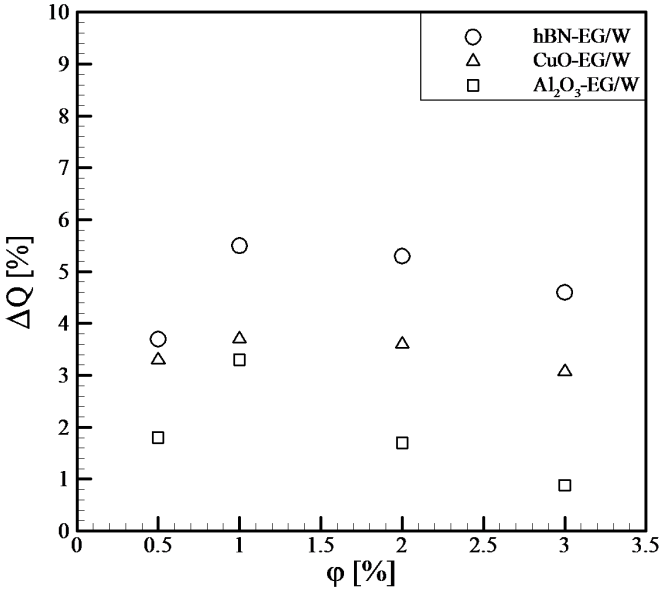

Figure 3.15. Flow rate reductions for same surface temperature of EG/W based Al_2O_3, CuO, and hBN nanofluids

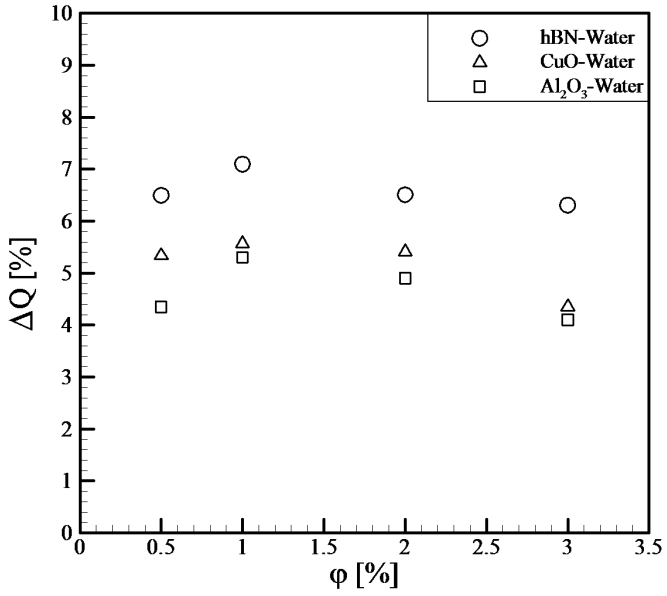

Figure 3.16. Flow rate reductions for same surface temperature of Water based Al_2O_3, CuO, and hBN nanofluids

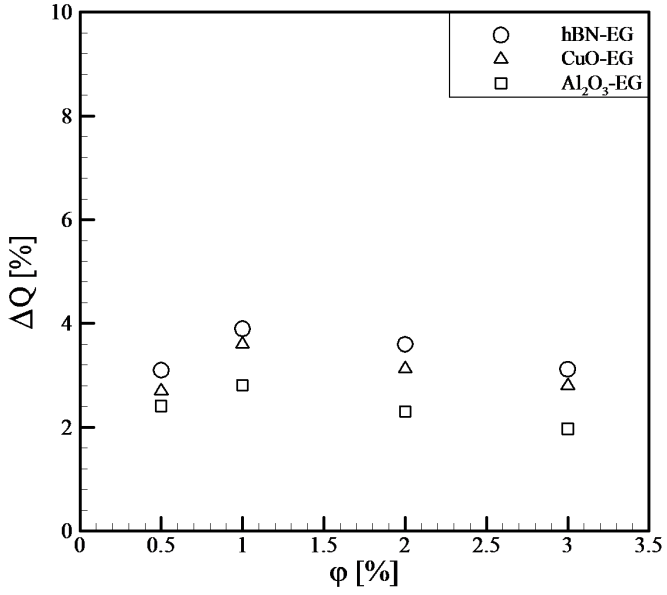

Figure 3.17. Flow rate reductions for same surface temperature of EG based Al_2O_3, CuO, and hBN nanofluids

It is observed that 1% concentration of the hBN nanofluid has the best combination of properties over the other fluids also for the pumping power increase for EG/W, water, and EG base fluids and the increments are 3.1%, 2.34% and, 3.12% for EG/W, water, and EG based nanofluids, respectively.

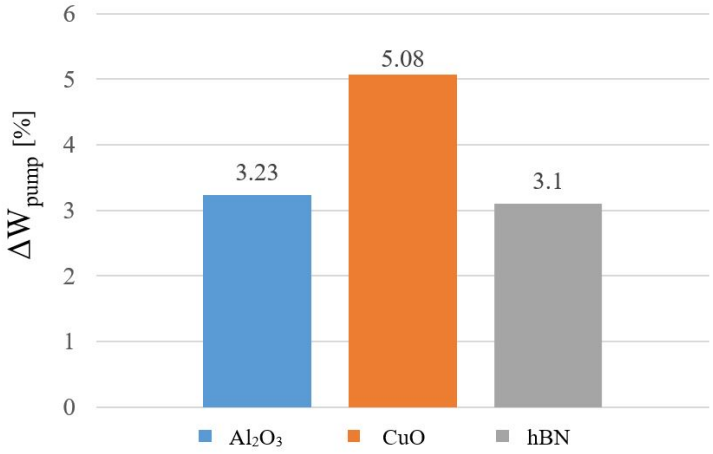

Figure 3.18. Pumping power increase for 1% particle concentration of EG/W based nanofluids concentration

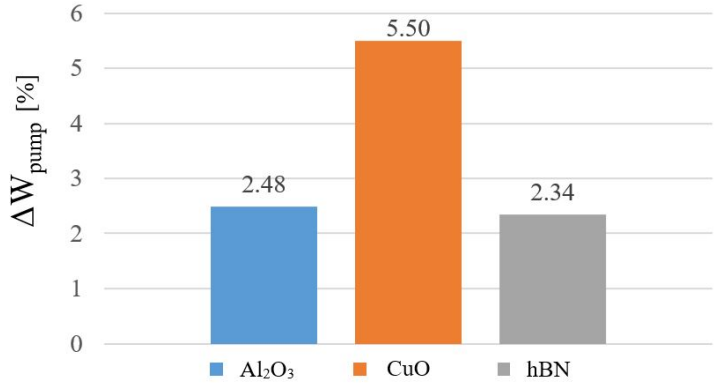

Figure 3.19. Pumping power increase for 1% particle concentration of Water based nanofluids concentration

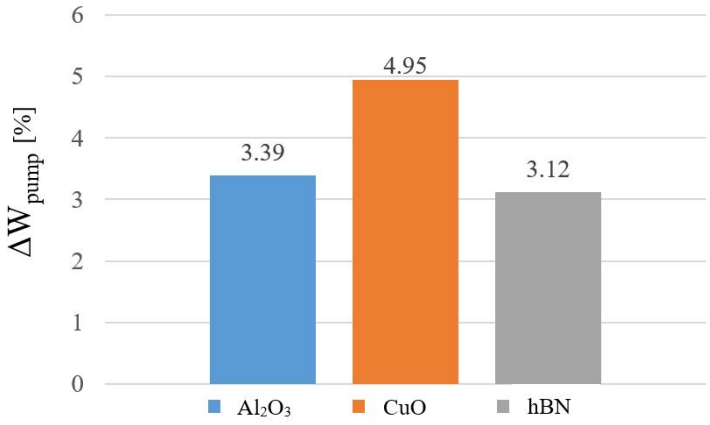

Figure 3.20. Pumping power increase for 1% particle concentration of EG based nanofluids concentration

3.2.3. Radiator Size Enhancement

It is observed that using nanofluid coolants improves overall cooling performance. Therefore, using nanofluids would enable using smaller sized radiators for the cooling system without compromising the system cooling performance. Smaller coolant systems result in smaller and lighter radiators, which would not only give some flexibility to the designers, but also help reduce the cost associated with the radiator. Therefore, it is worthwhile to investigate the opportunity of reducing the radiator size. Change in size of the radiator can be calculated by repeating the NTU effectiveness method for nanofluid coolants to achieve the system resistance same as when the base fluids are used. Total heat-transfer area, A_t , is able to be changed by altering the surface area of single fin. Due to adjusting the dimension of fin surface area, width of fins, D_f , can be regulated. After recalculating the system resistance with a specifed flow rate for EG/W base fluid in order to obtain same resistance with nanofluids, width of fins are adjusted. Change in size of the radiator that yields identical cooling performance can be defined as follows

$$R_A = 100\frac{A_{nf}(\varphi) - A_{bf}(0)}{A_{bf}(0)} \tag{3.5}$$

The maximum size reduction occurs as 11.4% for 1% concentration of hBN nanoparticles with EG/W base fluid. Since the thermal performance maximizes around 1% volume concentration of nanoparticles, size reductions of radiator are compared only for EG/W based nanofluids of 1% concentration. Figure 3.21 shows the radiator size reductions for EG/W based nanofluids.

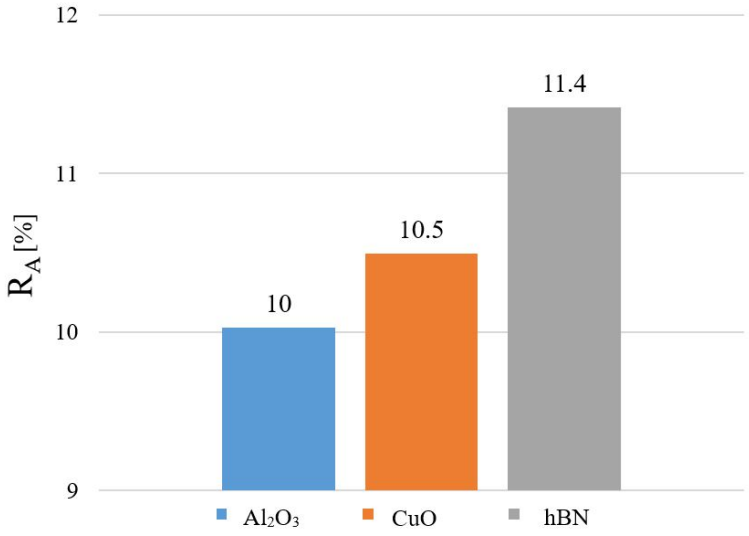

Figure 3.21. Radiator size reduction results for EG/W based Al_2O_3, CuO, and hBN nanofluids

4. CONCLUSION

4.1. Concluding Remarks

Thermal performance of nanofluid coolants in a cooling system 1.5 liter passenger car engine is examined in comparison with traditional coolants. Water, EG, and EG/W are considered as base fluids and nanofluids with CuO, Al_2O_3 and hBN nanoparticles for a particle volume fraction of 0.5-3% range are investigated at different volumetric flow rates. A cooling performance metric was defined in terms of resistance. According to results, nanofluids show superior heat-transfer capability than traditional coolants. The simulation results show that heat rejection increases for 3 nanoparticles and concentrations in between 0.5-3%. hBN nanofluids show higher performance with respect to the Al_2O_3 and CuO nanofluids. System resistance results of 1% particle concentration of EG/W based nanofluids are 0.386 K/W, 0.39 K/W and 0.392 K/W for hBN, CuO and Al_2O_3 nanoparticles, respectively. Engine block temperature decreases in the case of using nanofluids. hBN nanoparticles have the highest cooling capacity increase and quantitative results showed cooling performance increase up to 10.3%. The maximum temperature reduction is equal to 20.9 K for 1% concentration EG/W based hBN nanoparticle. As in the engine block, the nanofluids in the radiator allows higher heat-transfer ratios. However, engine resistance is the dominant component of system resistance therefore, radiator side thermal resistance effectuates a small portion of system thermal resistance. Aside from thermal analysis. Pressure drop calculations along pathway of nanofluid coolants for each case are executed. Resuls indicates pressure drop increases in the case of nanofluid use. Higher pressure drops increase the required pumping power up to 5.08% since the viscosity and the density of nanolufluids are increasing with particle concentration. Minimum increase of pumping power occurs for EG/W based hBN nanofluids since hBN has the best combination of properties. Minimum pumping power increase is 3.1%. 51 Required flow rates for nanofluid coolants to achieve maximum engine block temperature as same as when the base fluids are used are also estimated. It is observed that with the use of nanofluids, the system can operate with lower flow rates. It shows that nanofluids has a potential to decrease the

pump speed. The highest flow rate reduction occurs as 5.5% for 1% particle concentration of hBN nanoparticle. Morevover, water and EG based nanofluids were compared. Results showed that nanoparticles enhanced the thermal properties. The thermal conductivity increase of the water based nanofluids are relatively higher, with relatively less increase in viscosity with increasing particle volume fraction, with respect to that of EG/W or EG based nanofluids. Therefore, the increase in cooling capacity for water based nanofluids is higher than it is for EG or EG/W based nanofluids. The highest cooling capacity increase occurs as 11.6% for water based hBN nanoparticle of 1% particle concentration.Another advantage is using nanofluids would enable using smaller sized radiators.It is deduced that the higher cooling capacity leads reducing of the radiator sizes up to 11.5% for 1% particle concentration of hBN nanoparticle.

4.2. Future Work

Although the grid independence and validation study of computational model was executed for EG/W base fluid, experimental validation study is required for complete system and each components individually using an engine setup with the same technical specifications by replacing the coolant with nanofluids. Other segments of engines are needed to be investigated since this study only examine 1.5 liter passenger car engine. Engines with higher or smaller volumes, heavy duty engines or any specialized engines for various working conditions are wortwhile to be inspected and to move this study forward. Further investigations are required in order to clarify the promising enhancement point by comparing the results of nanofluids. Further examination procedure may include gathering and analysis of measurement data for a variety of different nanoparticles, concentrations and engine speed conditions in order to approve increased heat released rates and lower surface temperatures.

REFERENCES

1. Srivastava, S. and N. S. Chauhan, "Nanofluids: Effectual Analysis in Automotive Application", Technical report, SAE Technical Paper, 2014.

2. Goud, R. R., V. Dhiman, *et al.*, "Design and Development of Cylinder Block for High Power Density Diesel Engine using CAE/CFD Tools for a Tractor Engine with Integrated Approach", Technical report, SAE Technical Paper, 2013.

3. Chol, S., "Enhancing thermal conductivity of fluids with nanoparticles", *ASME-Publications-Fed*, Vol. 231, pp. 99–106, 1995.

4. Das, S. K., N. Putra, P. Thiesen, and W. Roetzel, "Temperature dependence of thermal conductivity enhancement for nanofluids", *Journal of Heat Transfer*, Vol. 125, No. 4, pp. 567–574, 2003.

5. Saripella, S., W. Yu, J. Routbort, D. France, and U. Rizwan, "Effects of nanofluid coolant in a class 8 truck engine", Technical report, SAE Technical Paper, 2007.

6. Bai, M., Z. Xu, and J. Lv, "Application of Nanofluids in Engine Cooling System", Technical report, SAE Technical Paper, 2008.

7. Liu, J., L. Zhou, M. Bai, Z. Xu, and J. Lv, "Study on the improvement of applying nanofluids to the heat load of sliding-contact component system (piston set and cylinder liner)", Technical report, SAE Technical Paper, 2008.

8. Leong, K., R. Saidur, S. Kazi, and A. Mamun, "Performance investigation of an automotive car radiator operated with nanofluid-based coolants (nanofluid as a coolant in a radiator)", *Applied Thermal Engineering*, Vol. 30, No. 17, pp. 2685–2692, 2010.

9. Peyghambarzadeh, S., S. Hashemabadi, S. Hoseini, and M. S. Jamnani, "Experimental study of heat transfer enhancement using water/ethylene glycol based nanofluids as a new coolant for car radiators", *International Communications in Heat and Mass Transfer*, Vol. 38, No. 9, pp. 1283–1290, 2011.

10. Huminic, G. and A. Huminic, "The cooling performances evaluation of nanofluids in a compact heat exchanger", Technical report, SAE Technical Paper, 2012.

11. Delavari, V. and S. H. Hashemabadi, "CFD simulation of heat transfer enhancement of Al 2 O 3/water and Al 2 O 3/ethylene glycol nanofluids in a car radiator", *Applied Thermal Engineering*, Vol. 73, No. 1, pp. 380–390, 2014.

12. Van Basshuysen, R. and F. Schaefer, "Modern engine technology from A to Z", Technical report, SAE Technical Paper, 2007.

13. Van Basshuysen, R. and F. Schäfer, *Internal combustion engine handbook-basics, components, systems and perspectives*, Vol. 345, 2004.

14. Aydogan, "Cooling performance investigation of nanofluids for internal combustion engine systems", *MS Thesis*, 2012.

15. Vatandas, "Boost modelling of Renault K9K 766 1.5l eu4 diesel engine and bench tests and comparison of experimental and calculation results", *MS Thesis*, 2012.

16. Chang, Y.-J. and C.-C. Wang, "A generalized heat transfer correlation for Iouver fin geometry", *International Journal of heat and mass transfer*, Vol. 40, No. 3, pp. 533–544, 1997.

17. Akbari, M., N. Galanis, and A. Behzadmehr, "Comparative assessment of single and two-phase models for numerical studies of nanofluid turbulent forced convection", *International Journal of Heat and Fluid Flow*, Vol. 37, pp. 136–146, 2012.

18. Behzadmehr, A., M. Saffar-Avval, and N. Galanis, "Prediction of turbulent forced convection of a nanofluid in a tube with uniform heat flux using a two phase approach", *International Journal of Heat and Fluid Flow*, Vol. 28, No. 2, pp. 211–219, 2007.

19. Hejazian, M., M. K. Moraveji, and A. Beheshti, "Comparative Numerical Investigation on TiO2/Water Nanofluid Turbulent Flow by Implementation of Single Phase and Two Phase Approaches", *Numerical Heat Transfer, Part A: Applications*, Vol. 66, No. 3, pp. 330–348, 2014.

20. Göktepe, S., K. Atalık, and H. Ertürk, "Comparison of single and two-phase models for nanofluid convection at the entrance of a uniformly heated tube", *International Journal of Thermal Sciences*, Vol. 80, pp. 83–92, 2014.

21. Heshmati, F. and H. Ertürk, "Single-phase models for improved estimation of friction factor for laminar nanofluid flow in pipes", *International Journal of Heat and Mass Transfer*, Vol. 95, pp. 416–425, 2016.

22. Choi, S., W. Yu, J. R. Hull, Z. Zhang, and F. Lockwood, "Nanofluids for vehicle thermal management", Technical report, SAE Technical Paper, 2001.

23. Bruggeman, V. D., "Berechnung verschiedener physikalischer Konstanten von heterogenen Substanzen. I. Dielektrizitätskonstanten und Leitfähigkeiten der Mischkörper aus isotropen Substanzen", *Annalen der physik*, Vol. 416, No. 7, pp. 636–664, 1935.

24. Hamilton, R. and O. Crosser, "Thermal conductivity of heterogeneous two-component systems", *Industrial & Engineering chemistry fundamentals*, Vol. 1, No. 3, pp. 187–191, 1962.

25. Koo, J. and C. Kleinstreuer, "A new thermal conductivity model for nanofluids", *Journal of Nanoparticle Research*, Vol. 6, No. 6, pp. 577–588, 2004.

26. Vajjha, R. S., *Measurements of thermophysical properties of nanofluids and computation of heat transfer characteristics*, Ph.D. thesis, University of Alaska Fairbanks, 2008.

27. İlhan, B., M. Kurt, and H. Ertürk, "Preperation and thermal conductivity of water based hBN nanofluids", *Proceedings of the 1st Thermal and Fluid Engineering Summer Conference, TFESC*, 2015.

28. Maxwell, J. C., *A treatise on electricity and magnetism*, Vol. 1, Clarendon press, 1881.

29. Choi, S. U., Z. G. Zhang, and P. Keblinski, "Nanofluids", *Encyclopedia of Nanoscience and Nanotechnology*, Vol. 6, pp. 757–773, American Scientific Publishers, 2004.

30. Einstein, A., "Über die von der molekularkinetischen Theorie der Wärme geforderte Bewegung von in ruhenden Flüssigkeiten suspendierten Teilchen", *Annalen der physik*, Vol. 322, No. 8, pp. 549–560, 1905.

31. Brinkman, H., "A calculation of the viscosity and the sedimentation constant for solutions of large chain molecules taking into account the hampered flow of the solvent through these molecules", *Physica*, Vol. 13, No. 8, pp. 447–448, 1947.

32. Murshed, S., K. Leong, and C. Yang, "Investigations of thermal conductivity and viscosity of nanofluids", *International Journal of Thermal Sciences*, Vol. 47, No. 5, pp. 560–568, 2008.

33. Corcione, M., "Empirical correlating equations for predicting the effective thermal conductivity and dynamic viscosity of nanofluids", *Energy Conversion and Management*, Vol. 52, No. 1, pp. 789–793, 2011.

34. Mishra, P. C., S. Mukherjee, S. K. Nayak, and A. Panda, "A brief review on viscosity of nanofluids", *International Nano Letters*, Vol. 4, No. 4, pp. 109–120, 2014.

35. Vajjha, R. S. and D. K. Das, "Experimental determination of thermal conductivity of three nanofluids and development of new correlations", *International Journal of Heat and Mass Transfer*, Vol. 52, No. 21, pp. 4675–4682, 2009.

36. İlhan, B., M. Kurt, and H. Ertürk, "Experimental investigation of heat transfer enhancement and viscosity change of hBN nanofluids", *Experimental Thermal and Fluid Science*, Vol. 77, pp. 272–283, 2016.

37. Handbook, A. F., "American society of heating, refrigerating and air-conditioning engineers", *Inc.: Atlanta, GA, USA*, 2009.

38. Freitas, C. J., "The issue of numerical uncertainty", *Applied mathematical modelling*, Vol. 26, No. 2, pp. 237–248, 2002.

APPENDIX A: VALIDATION STUDY

Actual fractional error indicates the difference between the surface temperatures obtained expeirmentally and calculated computationally. It is seen that actual fractional error, A_e, is 2.84% and in a good agreement with experimental data. Grid convergence was tested, after obtaining the surface temperature result which is in conformity with experimental data. Grid Convergence Index (GCI) is one of the most common grid refinement method it was proposed by Roache for the uniform reporting of grid convergence studies in CFD and related disciplines [38]. The method provides an objective asymptotic approach to quantification of uncertainty of grid convergence. The basic idea is to relate the results from any grid convergence test to the expected results. The GCI is based upon a grid convergence error estimator derived from the theory of generalized Richardson Extrapolation which is given in Eqs. A.1 and A.2 as follows

$$E = \frac{e}{r^p - 1} \tag{A.1}$$

$$e = \frac{f_2 - f_1}{f_1} \tag{A.2}$$

where f indicates the results of different grid solutions. Actual fractional error A_e can be defined as usual as follows

$$A_e = \frac{f_1 - f_{exact}}{f_{exact}} \tag{A.3}$$

where f_{exact} represents experimental result. The Grid Convergence Index is stated as an error percentage and provides a confidence bound on the estimated error band within which the numerically converged solution will probably lie. The GCI is a measure of the percentage the computed and it indicates an error band on how far the solution is from the asymptotic value. A small value of GCI indicates that the computation is within the asymptotic range and it can be used with a minimum of two mesh solutions.

The GCI for fine and coarse grid solutions are defined as follows

$$GCI_{12} = F_s \frac{|e|}{r^p - 1} \tag{A.4}$$

$$GCI_{23} = F_s \frac{|e|\, r^p}{r^p - 1} \tag{A.5}$$

where F_s is a factor of safety which is recommended to be Fs=3.0 for comparisons of two grids and Fs=1.25 for comparisons over three or more grids. The higher factor of safety is recommended for reporting purposes and is quite conservative of the actual errors. Subcriptions 1, 2, 3 stand for fine, medium and coarse grids and, 12 and 23 represent fine grid solution and coarse grid solution, respectively. p is the rate of convergence and if the solutions on three grids are exist, then the order of the rate of convergence of the discretization can be computed directly from the three solutions without a need for estimating the exact solution as follows

$$p = \ln\left(\frac{f_3 - f_2}{f_2 - f_1}\right) / \ln(r) \tag{A.6}$$

where r is grid refinement ratio. If the refinement and the grid are unstructured, there is no systematic grid refinement index, in such grid refinement studies r is defined in terms of the total number of elements used in the coarse and fine grids as follows

$$r = \left(\frac{N_1}{N_2}\right)^{(1/D)} \tag{A.7}$$

where N is the total number of nodes and D is the dimensionality of the flow domain. The asymptotic range of convergence can be checked by observing two GCI values as follows

$$GCI_{23} = r^p GCI_{12} \tag{A.8}$$

The magnitude of the fine and the coarse grid value of the Grid Convergence Index from Equation A.4 and Equation A.5 are 0.651 and 1.862, respectively. If the asymptotic range of convergence is checked by Equation A.8, it is seen that the result approximately 1 and indicates that the solutions are well within the asymptotic range of convergence. Value of maximum surface temperature estimated by Richardson Extrapolation is 755.32 K. Based on this study it can be concluded that the surface temperature of water jacket is estimated to be T = 755.2 K with an error band of approximately 0.09%.

Grid Convergence Index for fine and coarse grid, GCI_{12} and GCI_{23}, order of convergence, p, refinement ratio, r, number of nodes, Richardson Extrapolation error estimators which are used in method are given in Table A.1.

Table A.1. Grid Convergence Index parameters

$\mathbf{N}_1$	5889273	**p**	27.2
$\mathbf{N}_2$	4543665	**r**	1.1
$\mathbf{N}_3$	2522453	$\mathbf{E}_{12}$	0.003
f_1	755.1	$\mathbf{E}_{23}$	0.03
f_2	755.3	$\mathbf{e}_{12}$	0.0265
f_3	757.4	$\mathbf{e}_{23}$	0.278
$\mathbf{F}_s$	3	$\mathbf{GCI}_{12}$	0.0084
$\mathbf{A}_e$	2.84	$\mathbf{GCI}_{23}$	0.088

APPENDIX B: STREAMLINE CONTOURS

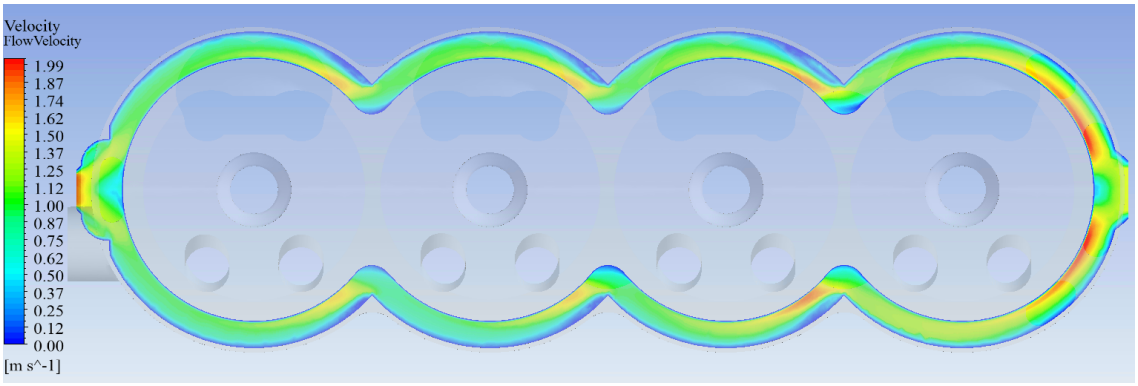

Figure B.1. Velocity distribution on cylinder block

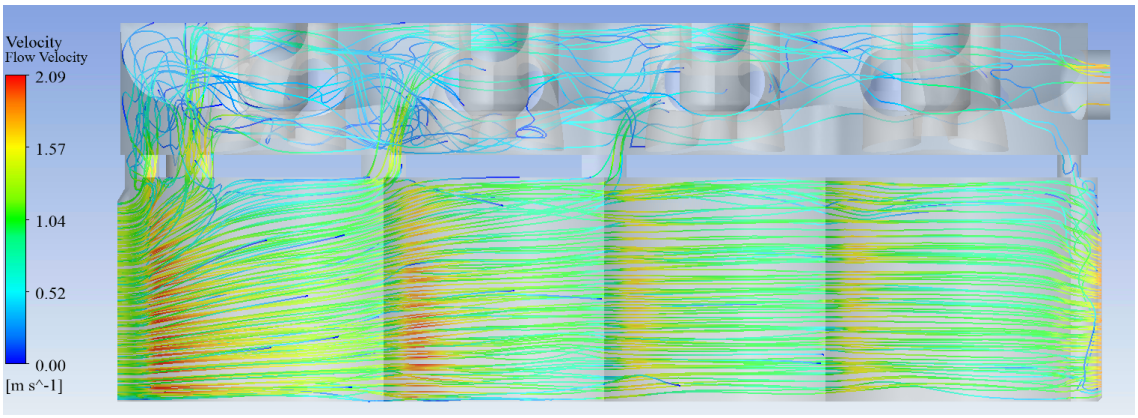

Figure B.2. Velocity streamline on engine block

APPENDIX C: THERMOPHYSICAL PROPERTIES

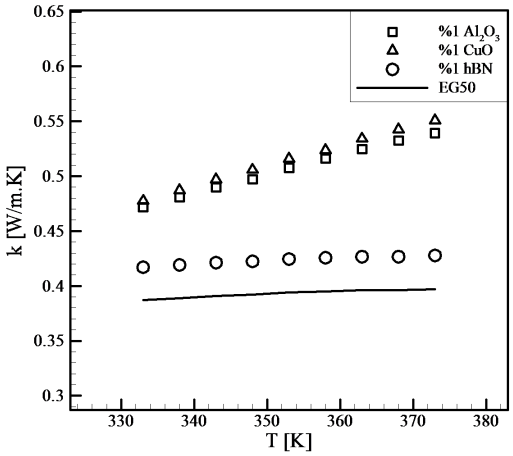

Figure C.1. Temperature dependent thermal conductivity of EG/W based nanofluids

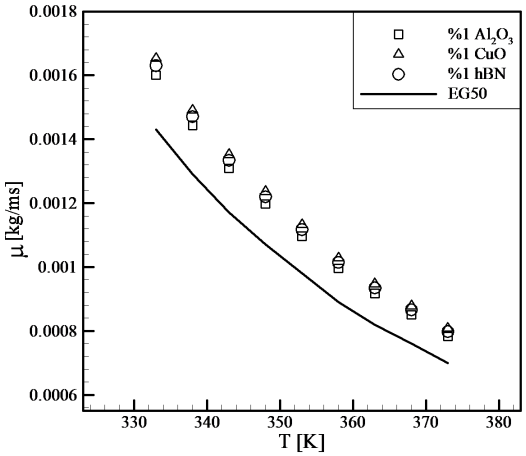

Figure C.2. Temperature dependent viscosity of EG/W based nanofluids

APPENDIX D: WATER JACKET MODEL

Technical drawings of water jacket model are submitted in following pages.

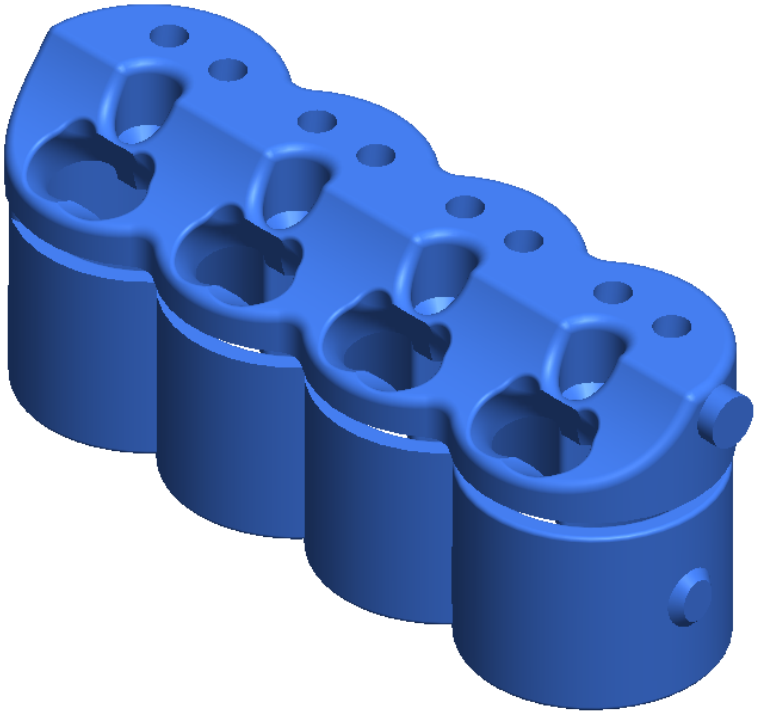

Figure D.1. Water jacket model

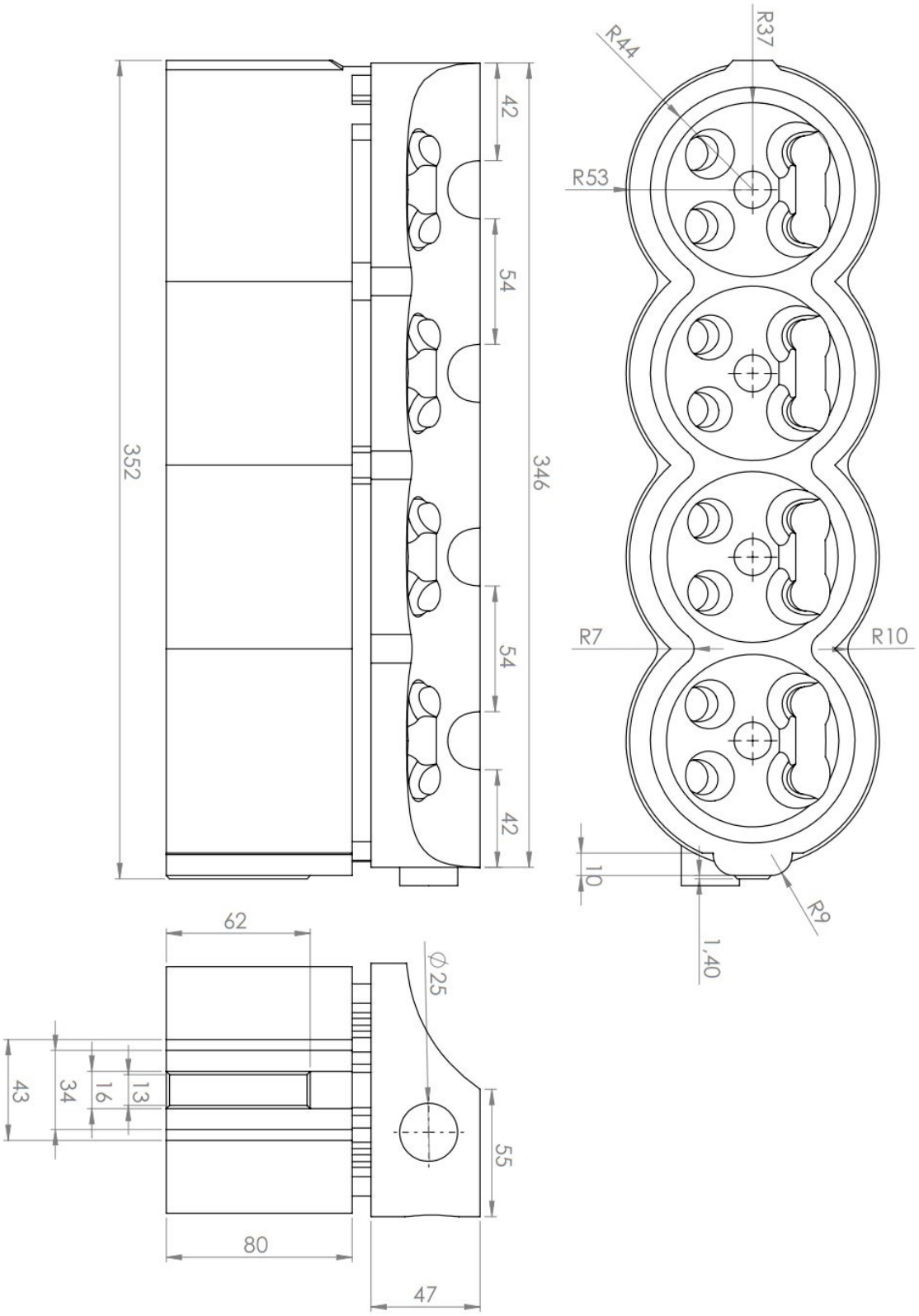

Figure D.2. Technical drawing of water jacket model

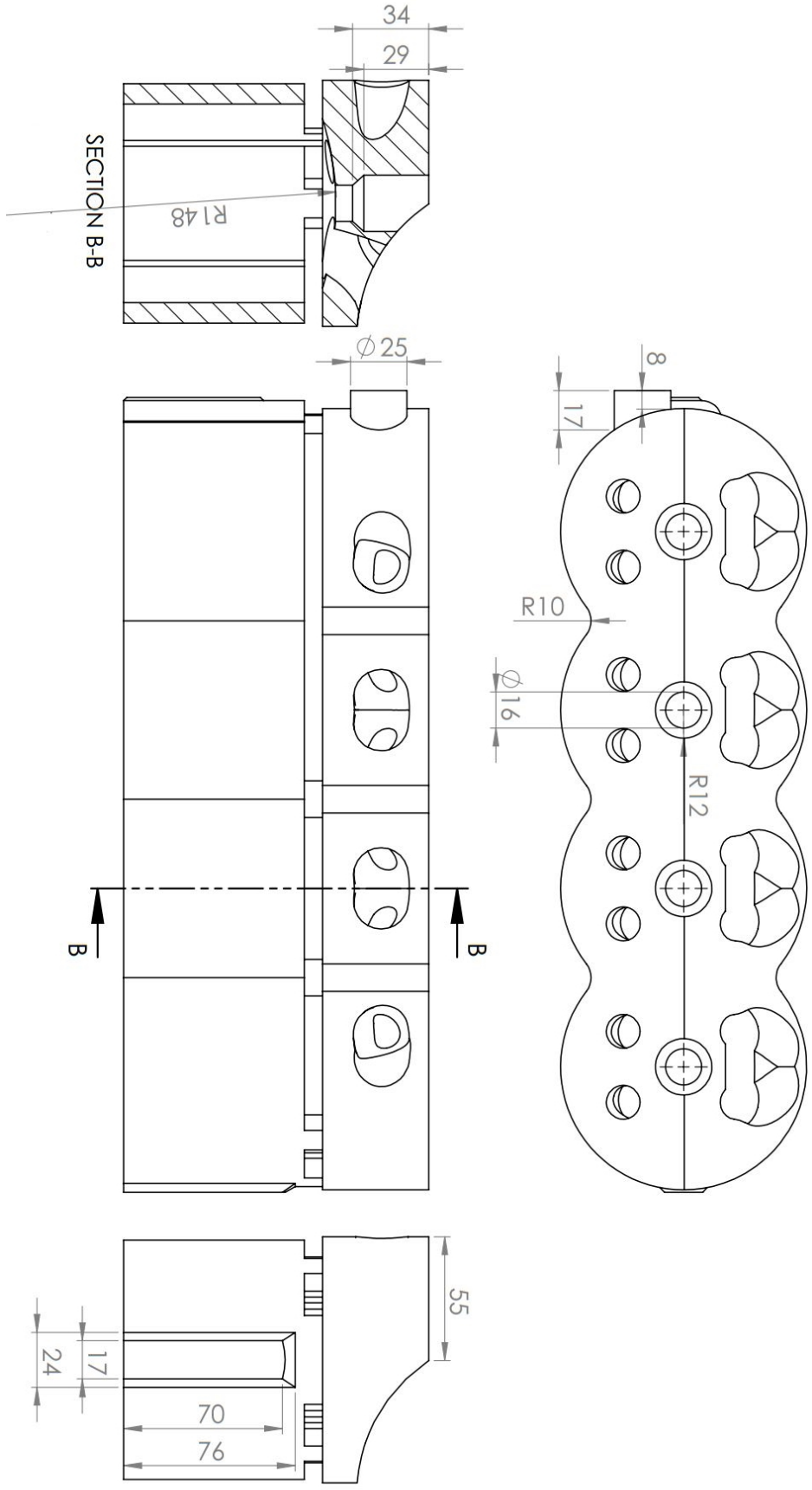

Figure D.3. Technical drawing of water jacket model

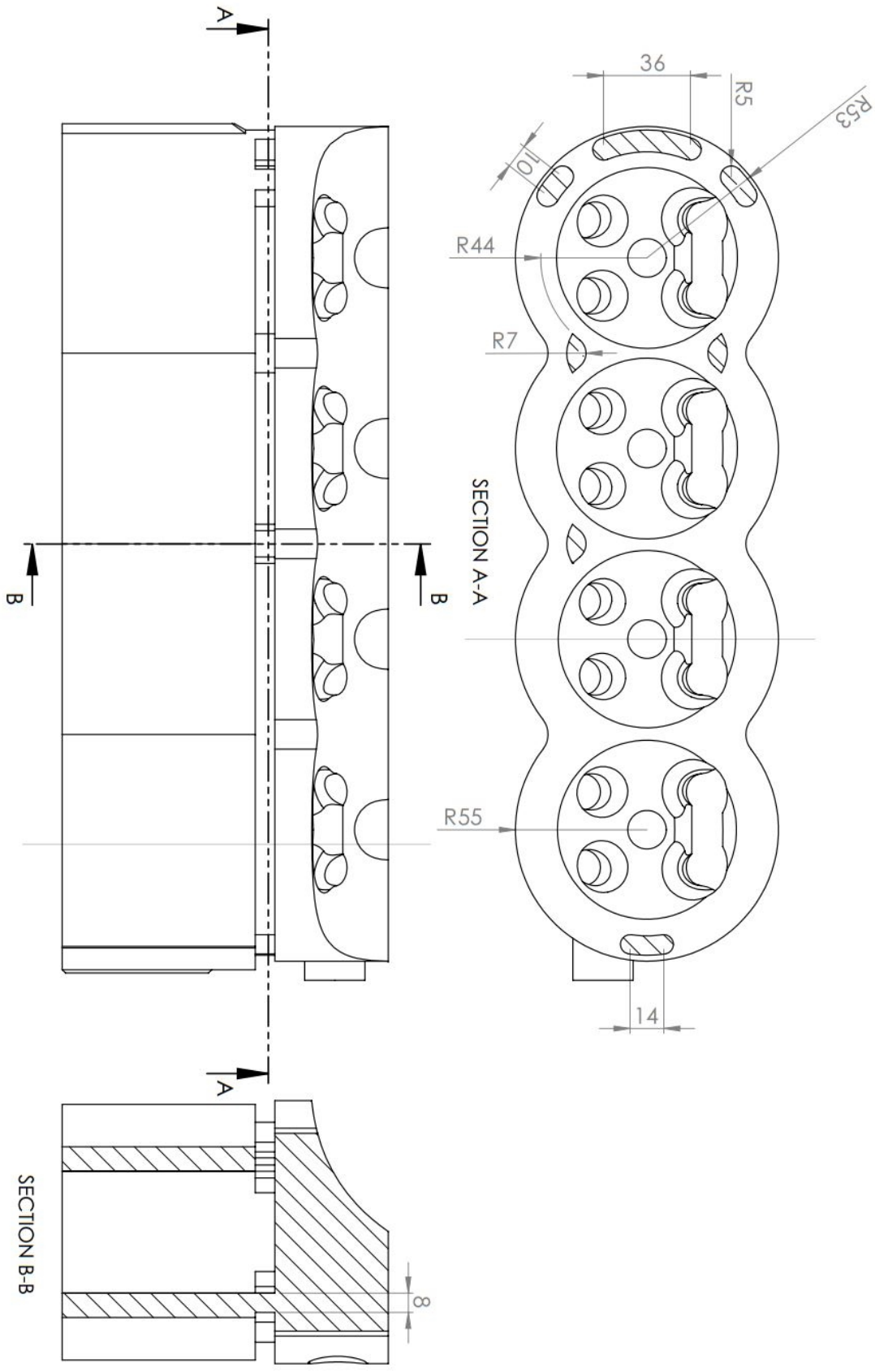

Figure D.4. Technical drawing of water jacket model